2. Materials and methods

2.1. Vector construction

The pMX-CH vector was constructed from the pMX vector (kindly provided by Dr. Kitamura, University of Tokyo) [2] by inserting the human IgG Cγ1 gene and the *Bacillus subtilis sacB* gene encoding levansucrase. In *Escherichia coli*, the expression of *sacB* in the presence of sucrose is lethal [11]. Briefly, the pCMVtag1 vector (Agilent technology) was modified at the multiple cloning site (MCS), and the *sacB* gene was inserted into the modified MCS (pCMVtag1-SacB) [12]. Constant region of human IgG cDNA was then inserted into the pCMVtag1-SacB vector. The DNA fragment containing the *sacB* and *Cγ* genes was removed from the pCMVtag1-CH vector by digestion with BamHI and NotI and was inserted into the pMX vector to construct the pMX-CH vector. To prepare the pMX-KmAmpR-TCR-Cα or Cβ vector, the ampicillin resistance gene (*AmpR*) from the pMX vector was first substituted with the kanamycin resistance gene (*KmR*) from the pCMVtag1 vector (Promega) (pMX-Km). The *AmpR* gene was amplified from pBR322 (Promega) by PCR and was then inserted into the BstXI site of the pMX-Km vector (pMX-KmAmpR). To prepare the DNA fragment containing the *sacB* gene and the constant region of TCRα (Cα) or TCRβ (Cβ), the Cα and Cβ cDNAs were amplified from human T cells by RT-PCR and were inserted into the NruI and NotI sites (pCMVtag1-Cα and pCMVtag1-Cβ, respectively) [13]. DNA fragments containing the *sacB*-Cα and *sacB*-Cβ genes were prepared from the pCMVtag1-Cα and pCMVtag1-Cβ plasmids and were inserted into the BamHI and NotI sites of the pMX-KmAmpR vector to construct the pMX-KmAmpR-TCR-Cα and Cβ vectors, respectively. Expression vectors for the human CD3γ, CD3δ, CD3ε, ζ and CD8 cDNAs were constructed by linking these cDNAs with the 2A sequence from the foot-and-mouth disease virus, as previously described (2A-hCD3-hCD8 vector) [14]. All human CD3γ, CD3δ, CD3ε, ζ and CD8 cDNAs were purchased from Origene.

2.2. Preparation of human peripheral blood lymphocytes and HLA typing

Human experiments were performed with the approval of the Ethical Committee at the University of Toyama. Informed consent was obtained from all subjects. Peripheral blood lymphocytes (PBLs) were isolated from heparinized blood samples by density gradient centrifugation using Ficoll-Hypaque (Immuno-Biological Laboratories). Screening for HLA-A24 haplotype positivity was performed by staining the PBLs with FITC-conjugated anti-HLA-A24 (MBL). The cells were then analyzed by flow cytometry.

2.3. Cell lines

RPMI 1640 and DMEM media (Wako Pure Chemical) were supplemented with 10% fetal bovine serum (Biowest), 100 μg/ml streptomycin and 100 U/ml penicillin. Human CD8 (hCD8)-expressing TG40 cells [15] were kindly provided by Dr. Ueno (Kumamoto University) with permission from Dr. Saito (Riken) and were maintained in RPMI 1640 medium. The retroviral packaging cell lines, PLAT-E and Phoenix-A, were kindly provided by Dr. Kitamura (University of Tokyo) and by Dr. G. Nolan (Stanford University), respectively, and were maintained in DMEM medium. The 2A-hCD3-hCD8-293T cells were established by transducing the 2A-hCD3-hCD8 vector into HEK293T cells (purchased from ATCC).

2.4. Antibody and MHC tetramer staining

EBV-specific T cells were stained with PE-conjugated HLA-A*2402/peptide tetramers. The amino acid sequences of the HLA-A*2402-restricted EBV peptides are as follows: TYPVLEEMF (BRLF-1 198-206), DYNFVKQLF (BMLF-1 320-328), IYVLVMLVL (LMP2 222-230), RYSIFFDYM (EBNA3A 246-254) and TYSAGIVQI (EBNA3B 217-225). All tetramers were purchased from MBL. The FITC-conjugated anti-human CD8 antibody (MBL), APC-conjugated anti-human CD3ε antibody (TONBO Biosciences), biotin-conjugated anti-murine CD3ε antibody (eBioscience) and APC-conjugated streptavidin (eBioscience) were used for flow cytometry.

2.5. Single-cell RT-PCR

Single-cell RT-PCR of the *TCR* gene from human T cells was performed using the single-cell 5′-RACE method as previously described [16]. The PCR products were analyzed by either direct sequencing or sequencing after subcloning into an expression vector. The TCR repertoire was analyzed using the IMGT/V-Quest tool (http://www.imgt.org/) [17].

2.6. Homologous recombination reaction in the competent cells

Homologous recombination in the competent cells was performed according to the instructions of the manufacturer (GENE BRIDGES). Briefly, competent cells harboring the pRedET expression plasmid were mixed with the pMX-KmAmpR-TCR-Cα or Cβ vector that was linearized by NruI digestion to remove *sacB* gene and the amplified cDNAs encoding TCR-Vα or Vβ, respectively. After transformation of the competent cells with the mixtures, the competent cells were streaked onto LB agar plates containing 4% sucrose and 100 μg/ml ampicillin. After incubation at 37 °C overnight, ampicillin-resistant *E. coli* cells were expanded. Plasmid DNAs were purified, digested with BamHI and NotI, and separated by agarose gel electrophoresis.

2.7. Retroviral transfection

The cDNAs encoding the TCR α or β chain were independently inserted into the pMX-KmAmpR-TCR-Cα or pMX-KmAmpR-TCR-Cβ plasmids, which were then transfected into the retroviral packaging cell line PLAT-E using FuGENE 6 (Roche). The culture supernatant from the transfected PLAT-E cells was collected 72 h after transfection and was added to hCD8-TG40 cells along with polybrene (Sigma–Aldrich). The transfection was monitored by the cell surface expression of murine CD3ε. For the retroviral transduction of the TCR cDNAs into 2A-hCD3-hCD8 293T cells, the recombinant retroviruses were produced using the packaging cell line Phoenix-A and infected with 2A-hCD3-hCD8 293T cells as described above.

3. Results

3.1. Undesirable homologous recombination between the 5′- and 3′-LTRs in the pMX retroviral vector

To insert cDNA fragments into the retroviral vector using homologous recombination, we first constructed a retroviral vector with the human IgG constant region (Cγ) and the *sacB* gene (Fig. 1A). For examining the cDNA insertion into the vector using homologous recombination, we amplified the V_H genes encoding human IgG V_H from single human B cells using the 5′-RACE method. The amplified V_H genes were mixed with the linearized vectors and introduced into the competent cells containing the pRED-ET plasmid [9], which induces homologous recombination in these

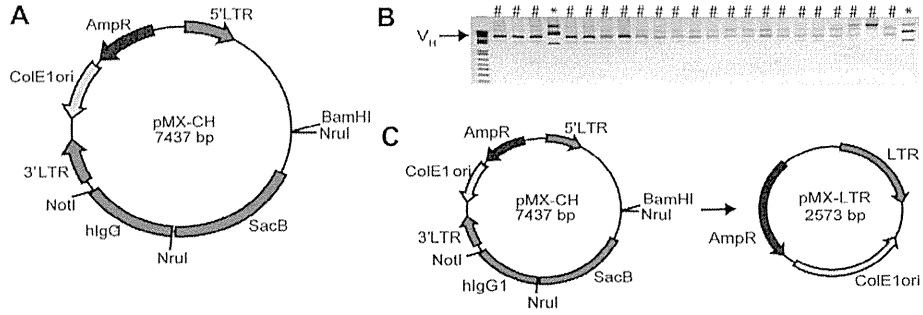

Fig. 1. Undesirable homologous recombination in the conventional retroviral pMX vector. (A) Map of the pMX-CH vector. The pMX-CH vector contains the *sacB* gene and the gene encoding the constant region of human IgG (B) Analysis of the homologous recombination products generated by the pMX-CH vectors. The PCR-amplified variable region of the antibody heavy chain (V_H) from human single B cells was inserted into the pMX-CH vector using homologous recombination. Plasmid DNA was prepared from the transformed colonies, digested with the BamHI and NotI restriction enzymes, and analyzed by agarose gel electrophoresis. The black arrow shows the target V_H gene. The asterisks indicate the pMX-CH vectors with the properly inserted V_H gene. "#" indicates vectors resulting from unsuccessful homologous recombination. (C) Scheme of unsuccessful homologous recombination in the pMX-CH vector. See the sequence analysis in Supplementary Fig. 1. The pMX-LTR results in the pMX- CH vector following unsuccessful homologous recombination.

cells [12]. The transformed cells were cultured on LB plates including ampicillin. Plasmid DNA from the ampicillin-resistant colonies was prepared, and the insertion of the V_H gene was examined by the restriction enzyme digestion. As shown in Fig. 1B, only 8% of the ampicillin-resistant cells contained pMX-Cγ vectors into which the V_H genes were properly inserted, whereas the rest of the colonies did not. Sequence analysis of the plasmid DNA that did not contain the V_H gene revealed that it only contained a single *LTR*, and the sequence between the 5′-LTR and 3′-LTR was deleted (Supplementary Fig. 1). These results demonstrated that homologous recombination preferentially occurred between the 5′- and 3′-LTRs of the pMX-C_H vectors, as illustrated in Fig. 1C.

3.2. Modification of the pMX retroviral vector for the insertion of DNA fragments using homologous recombination

In conventional retroviral vectors, *E. coli* selection markers, such as AmpR or KmR genes, are located adjacent to the *Col-E1* replication origin (*ori*). Consequently, homologous recombination between the 5′- and 3′-LTRs in these retroviral vectors resulted in the production of the vector shown in Supplementary Fig. 1. We assumed that the frequency of homologous recombination between the 5′- and 3′-LTRs was much higher than that of homologous recombination between the retroviral vectors and the target DNA fragments when the recombination reaction was conducted between linearized retroviral vectors and the target DNA fragments because the distance between the 5′- and 3′-LTRs is stochastically much shorter than the distance between the vector and the target DNA fragment.

To specifically select the *E. coli* cells that contained the retroviral vector into which the target DNA was properly inserted, we constructed a retroviral vector in which the *E. coli* selection marker gene was located adjacent to the insertion site of the target DNA fragment by homologous recombination (Fig. 2A). When we inserted the target DNA into the modified retroviral vector using homologous recombination, three possible products may be produced. When homologous recombination occurs between the 5′-LTR and 3′-LTR, the products (i) and (ii) in Fig. 2A will be produced. When homologous recombination properly occurs between the vector and the target DNA fragment, then product (iii) will be produced. Product (i) contains the *ori* but lacks the *AmpR* gene, and the *E. coli* harboring this product fail to grow in medium containing ampicillin. Product (ii) contains the *AmpR* gene but lacks the *ori*, and the *E. coli* harboring this product fail to grow in the medium because the plasmid DNA cannot be replicated. Only the *E. coli* harboring product (iii) can grow in the medium containing ampicillin, as this product contains both the *ori* and the *AmpR* gene. Therefore, we may obtain only the proper product (iii) through homologous recombination. According to this hypothesis, we inserted the *AmpR* gene into the pMX-Km vector, in which the ampicillin resistance gene was replaced with the kanamycin resistance gene at a site between the 3′-LTR and the multiple cloning site (pMX-KmAmpR) (Fig. 2B).

3.3. High-throughput cloning using the modified retroviral vectors with homologous recombination

To confirm the applicability of the vector for cloning by homologous recombination, we inserted the *sacB* gene and the constant region of either human TCRα or TCRβ into the vector (pMX-KmAmpR-TCR α/β) (Fig. 3A). We amplified the V region cDNA of either the TCRα or TCRβ gene from single human $CD8^+$ T cells using the 5′-RACE method (Fig. 3B) and inserted them into the *Nru*I-linearized pMX-KmAmpR-TCR α/β vector using homologous recombination, as described in Section 2. We picked the resultant ampicillin resistant colonies, grew them in medium containing ampicillin and prepared the plasmid DNA. We then digested the plasmid DNA with restriction enzymes to examine the proper insertion of the TCR Vα (TRAV) or Vβ (TRBV) cDNA. Of the ampicillin resistant cells, 100% and 81.3% of the competent cells contained the vectors in which the TRAV- and TRBV-cDNAs were properly inserted, respectively (Fig. 3C). These results showed that the pMX-KmAmpR-TCR α/β vectors enabled the efficient cloning of the TCR gene using homologous recombination.

3.4. Usefulness of the pMX-KmAmpR-TCR α/β vectors for the functional evaluation of the cloned TCR cDNAs in a high-throughput and comprehensive manner

To evaluate the usefulness of the vector for high-throughput cloning, we cloned the TCR genes from Epstein-Barr virus (EBV)-specific $CD8^+$ T cells derived from HLA-$A24^+$ latent healthy donors. We detected the EBV-specific $CD8^+$ T cells using a HLA-A*2402-restricted tetramer mixture of the five EB virus epitopes (BRLF-1, BMLF-1, LMP2, EBNA3A and EBNA3B) and then single-cell sorted the tetramer-positive cells from 10 donors whose frequencies of EBV tetramer-positive cells were more than 0.06% of the $CD8^+$ T-cell population. We amplified 444 pairs of TRAV and TRBV cDNAs from the sorted single cells using the 5′-RACE method and cloned the TCR α and β cDNAs into the pMX-KmAmpR-Cα or pMX-KmAmpR-Cβ vectors, respectively. Next, to determine the antigen-specificity of the cloned TCRs, we retrovirally transferred the

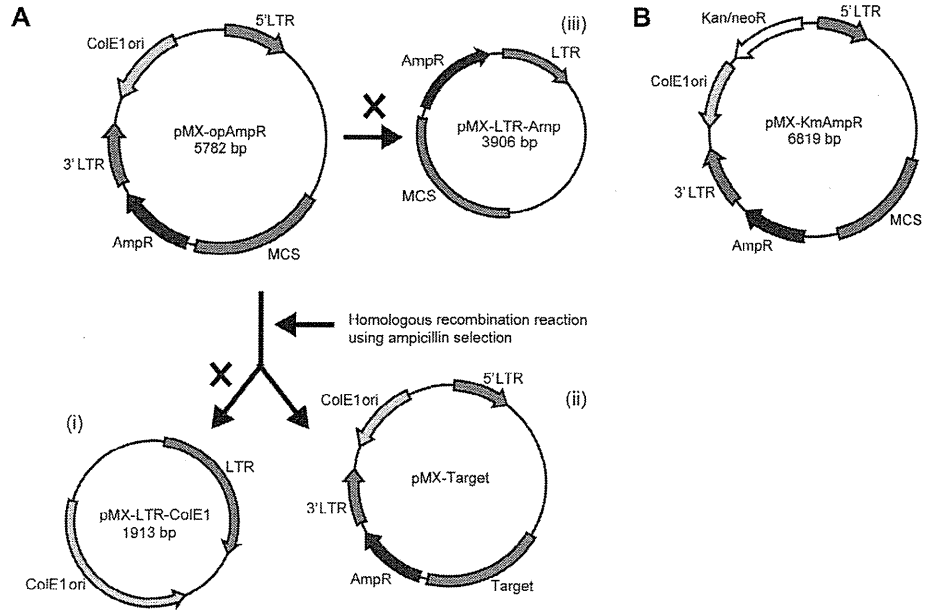

Fig. 2. Schematic illustration of the modified retroviral pMX vector. (A) Schematic illustration of the homologous recombination using the pMX-opAmp vector. (i) and (ii) Products of homologous recombination between the 5′- and 3′-LTRs. (iii) Product of homologous recombination between the target gene and the vector. (B) The pMX-Km vector contains the *AmpR* gene in the opposite position of the Col-E1 ori relative to two LTRs (pMX-KmAmpR).

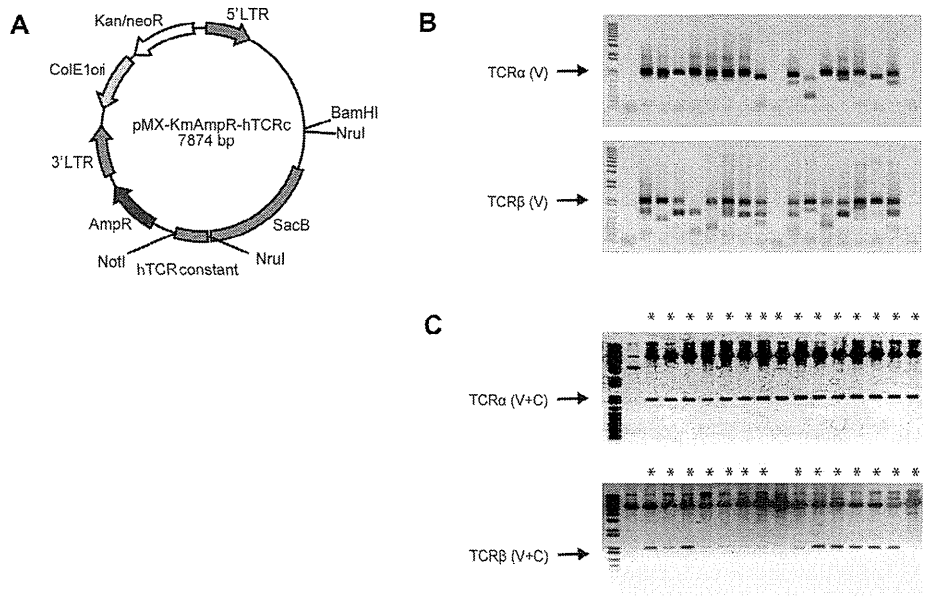

Fig. 3. Cloning of PCR-amplified cDNAs into the modified retroviral pMX vector through homologous recombination. (A) Schematic illustration of the modified pMX-KmAmpR vector for TCR cloning. (B) Amplified products of the variable regions of the TCRα or β genes from single human T cells. The amplified products were analyzed by agarose gel electrophoresis. Black arrow shows the target TCR-Vα (upper) or Vβ (lower). (C) Cloning of the PCR-amplified TCR-Vα or Vβ genes into the pMX-KmAmpR-TCR-Cα/Cβ using homologous recombination. The PCR-amplified TCR-Vα or Vβ were cloned into the pMX-KmAmpR-TCR-Cα or Cβ vectors using homologous recombination, respectively. Plasmid DNA was prepared from ampicillin-resistant colonies, digested with BamHI and NotI and separated by agarose gel electrophoresis. The black arrows show TCRα (upper) or TCRβ (lower), respectively. Asterisks indicate the plasmid that underwent successful homologous recombination.

TCR cDNAs into the TG40 cell line, which does not express endogenous TCR, and stained them using the EBVpep/HLA-A*2402 tetramer mixture. Ninety-five percent of the TCRs that were expressed on TG40 cells bound the tetramer (data not shown). The analysis of the cloned TCRs showed that the repertoire of the EBV-specific TCRs was highly restricted; in particular, Vβ5 was frequently used with TRBV (Fig. 4A). Furthermore, the number of T cell clones obtained from each donor was inversely correlated with the percentage of tetramer$^+$ CD8$^+$ T cells (Fig. 4B), suggesting that the specific clones were expanded in each donor to regulate EBV latency. During flow cytometric analysis, we found that some TCRs were hardly expressed on TG40 cells. The TG40 cells expressed only mouse CD3 molecules. We speculated that some human TCRs were difficult to associate with mouse CD3 molecules. To examine this possibility, we transduced two groups of human TCRs into the HEK293T-hCD3 cells that expressed human CD3 molecules: Ones that could be expressed on a large proportion of TG40 cells and ones that were hardly expressed on TG40 cells. Flow cytometric analysis (Fig. 4C) revealed that similar percentages of HEK 293T-hCD3 cells that were transduced with TCRs of each group

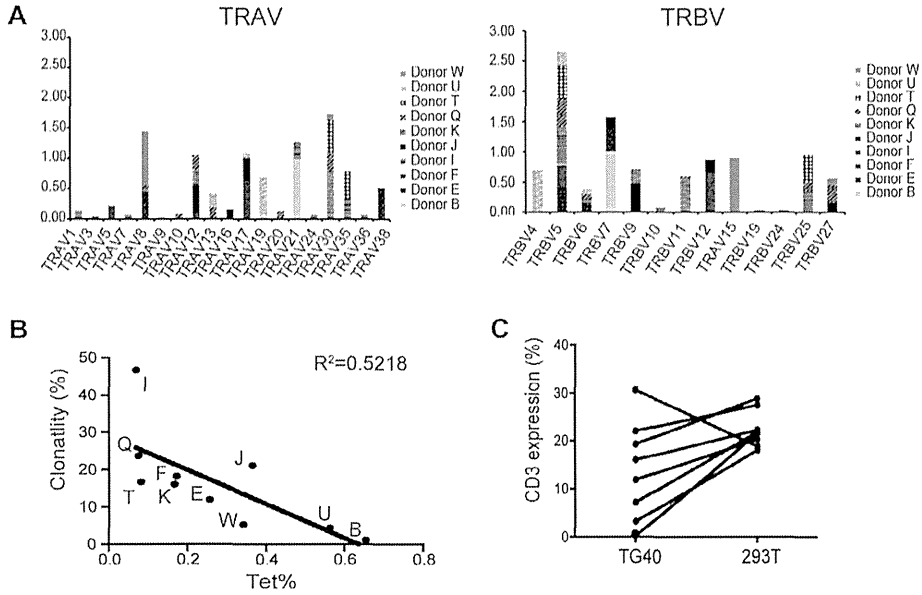

Fig. 4. Functional analysis of the cloned TCRs using the retroviral transduction method. (A) Comprehensive repertoire analysis of the EBV-specific TCRs from 10 latent healthy donors. The V regions of TCRα/β were obtained from single CD8$^+$ T cells that were stained with EBVpep/HLA-A*2402 tetramer mixture and were cloned into the pMX-KmAmpR-TCR-Cα/Cβ vectors using homologous recombination. The EBV-specificity of the cloned TCRα/β pairs was analyzed as described in Section 2. The frequency of the TCR repertoire (%) was calculated using the following formula: Frequency of TCR repertoire (%) = (the number of cloned TCR)/(the number of analyzed T cell clones) × 100. (B) Relationship between the number of cloned TCRs and the percentage of EBV-specific tetramer-positive cells in the CD8$^+$ T cells of 10 latent healthy donors. Clonality (%) was calculated using following formula: Clonality (%) = (the repertoire number)/(the number of analyzed T-cell clones) × 100. "R^2" shows the index correlation. The index correlation was calculated using the GraphPad Prism6 software. (C) Comparison of the cell surface expression of retrovirally-transduced TCRs. Representative TCRs of two groups: Ones that could be expressed on a large proportion of TG40 cells and ones that were hardly expressed on TG40 cells were transduced into 2A-hCD3-hCD8-293T cells and the cell surface expression of the TCRs was analyzed.

expressed human CD3 on the cell surface. The results showed that the expression of some human TCR molecules on the cell surface was affected by the species of the CD3 molecules.

4. Discussion

This study was performed to construct a retroviral vector in which the gene of interest can be inserted by homologous recombination and that is suitable for high-throughput cloning. Retroviral vectors contain 5′- and 3′-LTRs of more than 600 base pairs that exhibit sequence homology of more than 99%. Consequently, it is extremely difficult to insert a target gene into a retroviral vector because homologous recombination preferentially occurs between the LTRs rather than between the target gene and the vector [9,10]. To overcome this difficulty, we integrated the DNA replication origin *Col E1 ori* and the *E. coli* selection marker at opposite positions relative to the 5′- and 3′-LTRs. Because both elements are necessary for *E. coli* to grow, only *E. coli* that harbor a retroviral vector containing the properly inserted target DNA fragment can grow in the selection medium.

Using our modified retroviral vectors, we cloned 444 pairs of TRAV and TRBV cDNAs from EBV-specific CD8$^+$ T cells and analyzed their antigen-specificity and function [16]. Numerous studies on the TCR repertoire of antigen-specific T cells have been performed using conventional analysis methods, such as a FACS-based method with a panel of mAbs specific to each TCR β (TRB) V gene family product [18] or PCR-based methods with a panel of TRBV-specific primers [19,20]. Additionally, our group and others have reported a single cell RT-PCR protocol that allows for the simultaneous identification of the CDR3 α and CDR3 β transcripts of TCRs in human [13] and mice [21]. However, these protocols could not retrieve the TCR α/β pairs and analyze their functions, including antigen-specificity. In contrast, the retroviral vector reported here enabled the high-throughput and comprehensive cloning of TCRs using homologous recombination and efficient confirmation of the antigen-specificity of the cloned TCRs through retroviral transduction.

We used TG40 cells that expressed murine CD3 to analyze the human TCRs. It is worth noting that some human TCRs are difficult to express on the cell surface in association with the murine CD3 molecules, whereas they can be efficiently expressed on the cell surface in association with human CD3 molecules. The TCRα/β heterodimer is expressed in association with the CD3γ, CD3δ, CD3ε and ζ molecules [22,23]. A remarkable feature of the transmembrane domains of these receptor components is the presence of nine basic/acidic residues. Mutations of some of these polar residues resulted in a loss of receptor expression at the cell surface, demonstrating that these polar residues are essential for the expression of TCR-CD3 at the cell surface [24,25]. In contrast, our data showed that the V regions of the TCRα/β heterodimer also affected TCR-CD3 expression at the cell surface, at least in the case of the human TCR-murine CD3 complex.

In conclusion, target cDNA can be cloned into our modified retroviral vector using homologous recombination, making this vector a powerful tool for high-throughput cloning and the functional analysis of cDNA products.

5. Conflict of interest

E.K., H.K., T.O., M.H., and A.M., have a patent regarding the modified retroviral vector described in this work.

Acknowledgments

We would like to thank S. Hirota for technical assistance and K. Hata for secretarial work. The retroviral pMX vector and the PLAT-E cell line were kindly provided by T. Kitamura (University of Tokyo). The hCD8-expressing TG40 cell line was kindly provided by T. Ueno and C. Motozono (Kumamoto University), with permission from T. Saito (Riken), and the Phoenix-A cell line was kindly

provided by G. Nolan (Stanford University). This research was supported by Grants from the Hokuriku Innovation Cluster for Health Science and a Grant-in-Aid from the Ministry of Education, Culture, Sports, Science and Technology in Japan.

Appendix A. Supplementary data

Supplementary data associated with this article can be found, in the online version, at http://dx.doi.org/10.1016/j.bbrc.2014.01.049.

References

[1] H. Okayama, P. Berg, A cDNA cloning vector that permits expression of cDNA inserts in mammalian cells, Mol. Cell. Biol. 3 (1983) 280–289.
[2] T. Kitamura, Y. Koshino, F. Shibata, T. Oki, H. Nakajima, T. Nosaka, H. Kumagai, Retrovirus-mediated gene transfer and expression cloning: powerful tools in functional genomics, Exp. Hematol. 31 (2003) 1007–1014.
[3] M.A. Kay, J.C. Glorioso, L. Naldini, Viral vectors for gene therapy: the art of turning infectious agents into vehicles of therapeutics, Nat. Med. 7 (2001) 33–40.
[4] M. Onodera, D.M. Nelson, A. Yachie, G.J. Jagadeesh, B.A. Bunnell, R.A. Morgan, R.M. Blaese, Development of improved adenosine deaminase retroviral vectors, J. Virol. 72 (1998) 1769–1774.
[5] S.H. Kim, S.S. Yu, J.S. Park, P.D. Robbins, C.S. An, S. Kim, Construction of retroviral vectors with improved safety, gene expression, and versatility, J. Virol. 72 (1998) 994–1004.
[6] J. Wrammert, K. Smith, J. Miller, W.A. Langley, K. Kokko, C. Larsen, N.Y. Zheng, I. Mays, L. Garman, C. Helms, J. James, G.M. Air, J.D. Capra, R. Ahmed, P.C. Wilson, Rapid cloning of high-affinity human monoclonal antibodies against influenza virus, Nature 453 (2008) 667–671.
[7] T. Tiller, E. Meffre, S. Yurasov, M. Tsuiji, M.C. Nussenzweig, H. Wardemann, Efficient generation of monoclonal antibodies from single human B cells by single cell RT-PCR and expression vector cloning, J. Immunol. Methods 329 (2008) 112–124.
[8] M.D. Hamilton, A.A. Nuara, D.B. Gammon, R.M. Buller, D.H. Evans, Duplex strand joining reactions catalyzed by vaccinia virus DNA polymerase, Nucleic Acids Res. 35 (2007) 143–151.
[9] Y. Zhang, F. Buchholz, J.P. Muyrers, A.F. Stewart, A new logic for DNA engineering using recombination in *Escherichia coli*, Nat. Genet. 20 (1998) 123–128.
[10] Y. Zhang, J.P. Muyrers, G. Testa, A.F. Stewart, DNA cloning by homologous recombination in *Escherichia coli*, Nat. Biotechnol. 18 (2000) 1314–1317.
[11] P. Gay, D. Le Coq, M. Steinmetz, T. Berkelman, C.I. Kado, Positive selection procedure for entrapment of insertion sequence elements in gram-negative bacteria, J. Bacteriol. 164 (1985) 918–921.
[12] A. Jin, T. Ozawa, K. Tajiri, T. Obata, S. Kondo, K. Kinoshita, S. Kadowaki, K. Takahashi, T. Sugiyama, H. Kishi, A. Muraguchi, A rapid and efficient single-cell manipulation method for screening antigen-specific antibody-secreting cells from human peripheral blood, Nat. Med. 15 (2009) 1088–1092.
[13] T. Ozawa, K. Tajiri, H. Kishi, A. Muraguchi, Comprehensive analysis of the functional TCR repertoire at the single-cell level, Biochem. Biophys. Res. Commun. 367 (2008) 820–825.
[14] A.L. Szymczak, C.J. Workman, Y. Wang, K.M. Vignali, S. Dilioglou, E.F. Vanin, D.A. Vignali, Correction of multi-gene deficiency in vivo using a single 'self-cleaving' 2A peptide-based retroviral vector, Nat. Biotechnol. 22 (2004) 589–594.
[15] T. Ueno, H. Tomiyama, M. Fujiwara, S. Oka, M. Takiguchi, Functionally impaired HIV-specific CD8 T cells show high affinity TCR-ligand interactions, J. Immunol. 173 (2004) 5451–5457.
[16] E. Kobayashi, E. Mizukoshi, H. Kishi, T. Ozawa, H. Hamana, T. Nagai, H. Nakagawa, A. Jin, S. Kaneko, A. Muraguchi, A new cloning and expression system yields and validates TCRs from blood lymphocytes of patients with cancer within 10 days, Nat. Med. 19 (2013) 1542–1546.
[17] V. Giudicelli, D. Chaume, M.P. Lefranc, IMGT/V-QUEST, an integrated software program for immunoglobulin and T cell receptor V-J and V-D-J rearrangement analysis, Nucleic Acids Res. 32 (2004) W435–440.
[18] K. Bieganowska, P. Hollsberg, G.J. Buckle, D.G. Lim, T.F. Greten, J. Schneck, J.D. Altman, S. Jacobson, S.L. Ledis, B. Hanchard, J. Chin, O. Morgan, P.A. Roth, D.A. Hafler, Direct analysis of viral-specific CD8+ T cells with soluble HLA-A2/Ta11–19 tetramer complexes in patients with human T cell lymphotropic virus-associated myelopathy, J. Immunol. 162 (1999) 1765–1771.
[19] M. Saito, G.P. Taylor, A. Saito, Y. Furukawa, K. Usuku, J.N. Weber, M. Osame, C.R. Bangham, In vivo selection of T-cell receptor junctional region sequences by HLA-A2 human T-cell lymphotropic virus type 1 Ta11–19 peptide complexes, J. Virol. 75 (2001) 1065–1071.
[20] N. Eiraku, R. Hingorani, S. Ijichi, K. Machigashira, P.K. Gregersen, J. Monteiro, K. Usuku, S. Yashiki, S. Sonoda, M. Osame, W.W. Hall, Clonal expansion within CD4+ and CD8+ T cell subsets in human T lymphotropic virus type I-infected individuals, J. Immunol. 161 (1998) 6674–6680.
[21] P. Dash, J.L. McClaren, T.H. Oguin 3rd, W. Rothwell, B. Todd, M.Y. Morris, J. Becksfort, C. Reynolds, S.A. Brown, P.C. Doherty, P.G. Thomas, Paired analysis of TCRalpha and TCRbeta chains at the single-cell level in mice, J. Clin. Invest. 121 (2011) 288–295.
[22] R.D. Klausner, J. Lippincott-Schwartz, J.S. Bonifacino, The T cell antigen receptor: insights into organelle biology, Annu. Rev. Cell Biol. 6 (1990) 403–431.
[23] L.P. Kane, J. Lin, A. Weiss, Signal transduction by the TCR for antigen, Curr. Opin. Immunol. 12 (2000) 242–249.
[24] R.S. Blumberg, B. Alarcon, J. Sancho, F.V. McDermott, P. Lopez, J. Breitmeyer, C. Terhorst, Assembly and function of the T cell antigen receptor. Requirement of either the lysine or arginine residues in the transmembrane region of the alpha chain, J. Biol. Chem. 265 (1990) 14036–14043.
[25] T. Rutledge, P. Cosson, N. Manolios, J.S. Bonifacino, R.D. Klausner, Transmembrane helical interactions: zeta chain dimerization and functional association with the T cell antigen receptor, EMBO J. 11 (1992) 3245–3254.

OncoImmunology 3, e27258; January 2014; © 2014 Landes Bioscience

A novel system for cloning human TCRs

Cutting short the way to TCR-based anticancer therapy

Eiji Kobayashi[1], Hiroyuki Kishi[1,*], and Atsushi Muraguchi[1]

[1]Department of Immunology; Graduate School of Medicine and Pharmaceutical Sciences; University of Toyama; Toyama, Japan

Keywords: gene therapy, hTEC10, single-cell RT-PCR, T-cell receptor

T-cell receptor (TCR)-based gene immunotherapy has emerged as a promising approach for the treatment of multiple malignancies. We have recently reported an efficient system for the cloning and functional evaluation of TCR-coding cDNAs. This system, which we named hTEC10, allows for the determination of TCR antigen specificity in less than 10 days, and may therefore constitute a fast and powerful platform for the development of new TCR-based anticancer therapies.

T cell receptor (TCR)-based gene immunotherapy is a promising strategy for the treatment of various cancers. Despite its great potential, this approach is still limited to specific tumor-associated antigens (TAAs) and to patients bearing common MHC class I alleles. Generally, characterizing the genes that encode TAA-specific TCRs requires the establishment of TAA-specific T-cell clones, which can take up several months. Furthermore, the screening of large amounts of T-cell clones is laborious. Recently, we have developed a system that allows for the cloning of genes encoding TCR α/β pairs from single TAA-specific T cells and the functional analysis of their antigen-specificity in less than 10 d. We named this system hTEC10, for "human TCR efficient cloning system within 10 days" (**Fig. 1**).[1]

Using hTEC10, we obtained 73 and 126 α fetoprotein (AFP)-specific TCRα/β-coding cDNA pairs from 2 hepatocellular carcinoma patients who had been successfully treated with an AFP-targeting peptide vaccine. The sequencing of the TCR-coding genes revealed that 199 TCRα/β cDNA pairs were categorized into 3 and 4 cDNA clones, respectively. The functional characterization of 7 AFP-specific TCRs identified one (clone 1–14, obtained from a single T-cell clone out of 199 AFP-specific T-cell clones available) that mediated robust cytotoxic effects against target cells pulsed with AFP-derived peptides. This result suggests that T-cell clones bearing high-affinity TAA-specific TCRs are very rare even among the peripheral blood lymphocytes of patients who had been successfully treated by TAA-targeting vaccines. Using conventional methods, minor T-cell populations such as clone 1–14 would be lost during culture, since large T-cell populations would take over and expand preferentially. Thus, our method is suitable for exploring very small populations of antigen-specific T cells that conventional screening methods may overlook, significantly increasing the possibility to obtain optimal TCR-coding cDNAs for TCR-based gene therapy.

Until recently, numerous studies on the TCR repertoire of antigen-specific T cells have been performed by flow cytometry, based on a panel of monoclonal antibodies specific for TCR β variable fragment (TRBV),[2] or by PCR-based methods, using a panel of TRBV-specific primers.[3] These methods characterize the TRBV regions of TCRs at the population level, but fail to provide insights into the TCR α variable fragments (TRAVs) as well as into the TRBV regions at a single-cell level. Thus, so far we have not been able to measure the true extent of the clonal diversity within $CD8^+$ cytotoxic T lymphocyte (CTL) populations isolated from cancer patients. In this context, we and others had reported single-cell RT-PCR protocols that permit the simultaneous characterization of the sequences encoding complementarity-determining region 3 (CDR3) α and β in human[4] and mouse[5] TCRs. However, these protocols cannot identify TCR α/β pairs, confirm their antigen specificity nor examine their ability to promote cytotoxic effector functions. In contrast, the hTEC10 system may provide us with a new way to analyze the TCR repertoire, as it supplies information of both the TCR α and β chains at the single-cell level and can assess their functional profile. In addition, hTEC10 may provide a useful means to assess the efficacy of anticancer vaccination.

For cancer immunotherapy to be efficient, hence resulting in tumor eradication in vivo, cytotoxic T cells expressing a TCR of sufficiently high avidity are required. In this context, Johnson and colleagues selected CTLs that displayed TAA-specific TCRs with sufficient affinity to induce tumor regression among more than 600 different TAA-specific T cells.[6] To obtain T cells with a sufficient avidity to eliminate tumors in vivo, Nauerth and collaborators have recently developed a new assay based on reversible MHC streptamers, allowing for the assessment of the dynamic dissociation

*Correspondence: Hiroyuki Kishi; Email: immkishi@med.u-toyama.ac.jp
Submitted: 11/18/2013; Accepted: 11/18/2013; Published Online: 01/01/2014
Citation: Kobayashi E, Kishi H, Muraguchi A. A novel system for cloning human TCRs: Cutting short the way to TCR-based anticancer therapy. OncoImmunology 2013; 2:e27258; http://dx.doi.org/10.4161/onci.27258

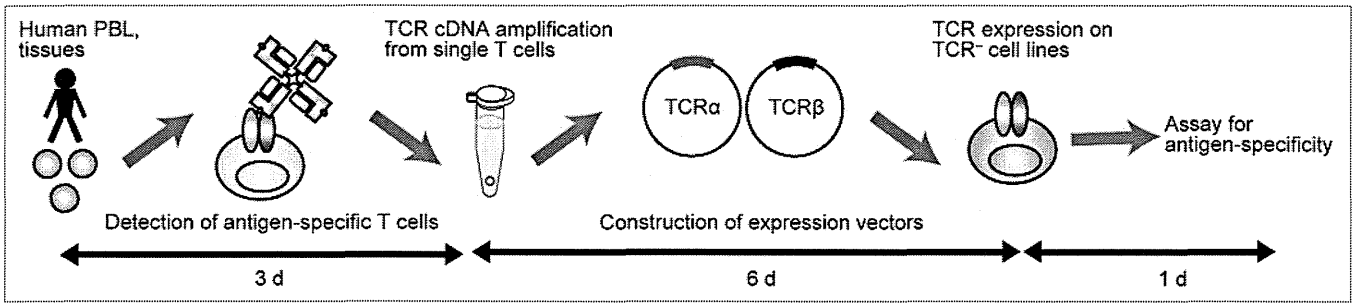

Figure 1. The hTEC10 system. Briefly, the cDNAs coding for human T-cell receptor (TCR) α and β chain are amplified from single T cells and cloned into an expression vector, which is then used to transduce the TCR⁻ T-cell line TG40. The antigen specificity of the TCR can be assessed by staining TCR-expressing TG40 cells with MHC tetramers or by monitoring CD69 expression. Of note, the entire procedure can be performed in less than 10 d. Reproduced with permissions from ref. 1.

(K_{off} rate) of fluorescently labeled, peptide-loaded MHC class I monomers from TCRs expressed on the surface of living T cells.[7] The assay enables a simple, quantitative and reproducible measurement of the K_{off} rate as a reliable indicator of TCR binding avidity. The combination of the hTEC10 system with this new method may provide us with a valuable approach to selectively retrieve high-affinity T-cell clones for TCR-based gene therapy. Another possible strategy to generate high-affinity TCRs is the genetic alteration of TCR-coding genes. Preliminary clinical trials have already demonstrated that genetically enhanced TCRs can indeed confer improved on-target effector functions to T cells. In this scenario, the hTEC10 system might also contribute by supplying several TCR-coding sequences as starting point for genetic engineering.

Concerning the adverse effect of high-avidity TCRs, 2 patients receiving affinity-enhanced melanoma antigen family A3 (MAGEA3)-specific T cells have recently died owing to the cross-reaction of adoptively transferred lymphocytes with a protein expressed in the pulsating cardiac tissue.[8] Furthermore, T cells expressing TCRs whose affinity is much higher than the physiological one have been shown to mediate increased off-target activity at the expenses of on-target effector functions.[9] Thus, methods are needed that allow for refining the affinity/avidity of TCRs to optimal levels, ensuring robust on-target effector functions in the absence of severe side effects.

Finally, in combination with MHC multimer-based staining protocols, the hTEC10 system can detect and retrieve TCR α/β cDNA pairs from $CD8^+$ T cells that secrete specific cytokines or express the activation marker tumor necrosis factor receptor superfamily, member 9 (TNFRSF9, best known as CD137 or 4–1BB) upon stimulation with antigenic peptides. Our findings indicate that the hTEC10 system can be used to isolate T cells from cancer patients without the identification of the corresponding TAAs. Briefly, T cells are stimulated with cancer cells followed by the isolation of interferon γ (IFNγ)-secreting or CD137-expressing $CD8^+$ T cells. Once the TCR-coding sequences of these cells are cloned, their antigen-specificity can be examined by analyzing the response of TCR-transduced T cells against malignant cells. This protocol extends the applicability of the hTEC10 system from the cloning of TCRs with known antigen specificity to the retrieval of TCRs of unknown antigen specificity. In conclusion, the hTEC10 system may provide a fast and powerful approach for the development of novel paradigms of TCR-based gene therapy against cancer.

Disclosure of Potential Conflicts of Interest

Authors have applied a patent of hTEC10 system.

References

1. Kobayashi E, Mizukoshi E, Kishi H, Ozawa T, Hamana H, Nagai T, Nakagawa H, Jin A, Kaneko S, Muraguchi A. A new cloning and expression system yields and validates TCRs from blood lymphocytes of patients with cancer within 10 days. Nat Med 2013; 19:1542-6; http://dx.doi.org/10.1038/nm.3358; PMID:24121927
2. Bieganowska K, Höllsberg P, Buckle GJ, Lim DG, Greten TF, Schneck J, Altman JD, Jacobson S, Ledis SL, Hanchard B, et al. Direct analysis of viral-specific CD8+ T cells with soluble HLA-A2/Tax11-19 tetramer complexes in patients with human T cell lymphotropic virus-associated myelopathy. J Immunol 1999; 162:1765-71; PMID:9973440
3. Eiraku N, Hingorani R, Ijichi S, Machigashira K, Gregersen PK, Monteiro J, Usuku K, Yashiki S, Sonoda S, Osame M, et al. Clonal expansion within CD4+ and CD8+ T cell subsets in human T lymphotropic virus type I-infected individuals. J Immunol 1998; 161:6674-80; PMID:9862696
4. Ozawa T, Tajiri K, Kishi H, Muraguchi A. Comprehensive analysis of the functional TCR repertoire at the single-cell level. Biochem Biophys Res Commun 2008; 367:820-5; http://dx.doi.org/10.1016/j.bbrc.2008.01.011; PMID:18191637
5. Dash P, McClaren JL, Oguin TH 3rd, Rothwell W, Todd B, Morris MY, Becksfort J, Reynolds C, Brown SA, Doherty PC, et al. Paired analysis of TCRα and TCRβ chains at the single-cell level in mice. J Clin Invest 2011; 121:288-95; http://dx.doi.org/10.1172/JCI44752; PMID:21135507
6. Johnson LA, Morgan RA, Dudley ME, Cassard L, Yang JC, Hughes MS, Kammula US, Royal RE, Sherry RM, Wunderlich JR, et al. Gene therapy with human and mouse T-cell receptors mediates cancer regression and targets normal tissues expressing cognate antigen. Blood 2009; 114:535-46; http://dx.doi.org/10.1182/blood-2009-03-211714; PMID:19451549
7. Nauerth M, Weißbrich B, Knall R, Franz T, Dössinger G, Bet J, Paszkiewicz PJ, Pfeifer L, Bunse M, Uckert W, et al. TCR-ligand koff rate correlates with the protective capacity of antigen-specific CD8+ T cells for adoptive transfer. Sci Transl Med 2013; 5:192ra87; http://dx.doi.org/10.1126/scitranslmed.3005958; PMID:23825303
8. Linette GP, Stadtmauer EA, Maus MV, Rapoport AP, Levine BL, Emery L, Litzky L, Bagg A, Carreno BM, Cimino PJ, et al. Cardiovascular toxicity and titin cross-reactivity of affinity-enhanced T cells in myeloma and melanoma. Blood 2013; 122:863-71; http://dx.doi.org/10.1182/blood-2013-03-490565; PMID:23770775
9. Schmid DA, Irving MB, Posevitz V, Hebeisen M, Posevitz-Fejfar A, Sarria JC, Gomez-Eerland R, Thome M, Schumacher TN, Romero P, et al. Evidence for a TCR affinity threshold delimiting maximal CD8 T cell function. J Immunol 2010; 184:4936-46; http://dx.doi.org/10.4049/jimmunol.1000173; PMID:20351194

PLOS ONE

Systemic CD8$^+$ T Cell-Mediated Tumoricidal Effects by Intratumoral Treatment of Oncolytic Herpes Simplex Virus with the Agonistic Monoclonal Antibody for Murine Glucocorticoid-Induced Tumor Necrosis Factor Receptor

Mikiya Ishihara[1], Naohiro Seo[1]*, Jun Mitsui[2], Daisuke Muraoka[1], Maki Tanaka[3], Junichi Mineno[3], Hiroaki Ikeda[1], Hiroshi Shiku[1]*

1 Department of Immuno-Gene Therapy, Mie University Graduate School of Medicine, Mie, Japan, **2** Department of Gastroenterological Surgery II, Hokkaido University Graduate School of Medicine, Hokkaido, Japan, **3** Gene Medicine Business Unit, Takara Bio Inc., Shiga, Japan

Abstract

Oncolytic virotherapy combined with immunomodulators is a novel noninvasive strategy for cancer treatment. In this study, we examined the tumoricidal effects of oncolytic HF10, a naturally occurring mutant of herpes simplex virus type-1, combined with an agonistic DTA-1 monoclonal antibody specific for the glucocorticoid-induced tumor necrosis factor receptor. Two murine tumor models were used to evaluate the therapeutic efficacies of HF10 virotherapy combined with DTA-1. The kinetics and immunological mechanisms of DTA-1 in HF10 infection were examined using flow cytometry and immunohistochemistry. Intratumoral administration of HF10 in combination with DTA-1 at a low dose resulted in a more vigorous attenuation of growth of the untreated contralateral as well as the treated tumors than treatment with either HF10 or DTA-1 alone. An accumulation of CD8$^+$ T cells, including tumor- and herpes simplex virus type-1-specific populations, and a decrease in the number of CD4$^+$ Foxp3$^+$ T regulatory cells were seen in both HF10- and DTA-1-treated tumors. Studies using Fc-digested DTA-1 and Fcγ receptor knockout mice demonstrated the direct participation of DTA-1 in regulatory T cell depletion by antibody-dependent cellular cytotoxicity primarily via macrophages. These results indicated the potential therapeutic efficacy of a glucocorticoid-induced tumor necrosis factor receptor-specific monoclonal antibody in oncolytic virotherapy at local tumor sites.

Citation: Ishihara M, Seo N, Mitsui J, Muraoka D, Tanaka M, et al. (2014) Systemic CD8$^+$ T Cell-Mediated Tumoricidal Effects by Intratumoral Treatment of Oncolytic Herpes Simplex Virus with the Agonistic Monoclonal Antibody for Murine Glucocorticoid-Induced Tumor Necrosis Factor Receptor. PLoS ONE 9(8): e104669. doi:10.1371/journal.pone.0104669

Editor: Claude Krummenacher, University of Pennsylvania School of Veterinary Medicine, United States of America

Received April 30, 2014; **Accepted** July 11, 2014; **Published** August 8, 2014

Data Availability: The authors confirm that all data underlying the findings are fully available without restriction. All relevant data are within the paper and its Supporting Information files.

Funding: This work was supported by grants from Ministry of Education, Culture, Sports, Science and Technology of Japan (24390300 and 24800033). The funders had no role in study design, data collection and analysis, decision to publish, or preparation of the manuscript.

Competing Interests: The authors have declared that no competing interests exist. Specifically, the following co-authors: M. Tanaka and J. Mineno confirm that, in spite of them being employed by commercial companies Takara Bio Inc., this does not alter the authors' adherence to all the PLOS ONE policies on sharing data and materials and that they are entitled and allowed to publish the results reported in this manuscript. H. Shiku is a PLOS ONE Editorial Board member. This does not alter the authors' adherence to PLOS ONE Editorial policies and criteria.

* Email: seo-naohiro@clin.medic.mie-u.ac.jp (NS); shiku@clin.medic.mie-u.ac.jp (HS)

Introduction

Oncolytic virotherapy has existed for over 100 years and is a promising method for the treatment of cancer patients because of the strong cytolytic response of virus-infected tumor cells; however, complications may result from the use of oncolytic viruses including toxicity against normal cells [1–3]. Thus, artificially modified oncolytic viruses have been engineered to achieve low toxicity against normal tissues together with sufficient antitumor activity. Oncolytic viruses that have been modified to express human cytokines, such as granulocyte macrophage colony-stimulating factor (GM-CSF) have the potential for future therapeutic use in the treatment of solid tumors. JX-594 is a GM-CSF-armed oncolytic poxvirus that has shown promising outcomes when administered by either intratumoral (i.t.) injection or intravenous (i.v.) infusion [4–8]. OncoVEX$^{GM\text{-}CSF}$ is an oncolytic virus based on the JS-1 strain of herpes simplex virus type-1 (HSV-1) that has been engineered to express human GM-CSF [9–12]. The results of a phase III trial demonstrate that melanoma patients treated with this virus show statistically significant improvement with durable responses [12].

HSV infection in wide ranges of cell populations results in degenerative change and death [13]. HF10 is a spontaneous mutant of HSV-1 strain HF [14] that lacks neuroinvasiveness and is at least 10,000-fold less virulent than wild-type HSV-1 in mice [15]. In several clinical studies of cancer patients, HF10 has been shown to have antitumor effects [16–19]. In murine studies, HF10 packaged with a GM-CSF-expressing amplicon has been reported to exhibit more tumoricidal activity than intact HF10 [20,21], supporting the hypothesis that HF10 exhibits maximal antitumor activity when used in combination with immunomodulators.

Glucocorticoid-induced tumor necrosis factor receptor (GITR) is a type I transmembrane protein of the tumor necrosis factor receptor family, and is involved in the regulation of T-cell receptor-mediated cell death [22]. GITR is similar to programmed cell death-1 (PD-1) and cytotoxic T-lymphocyte antigen 4 (CTLA-4), both of which have been applied clinically as immune modifiers in tumor therapy [23]. GITR has been reported to be expressed at high levels on $CD4^+$ $CD25^+$ regulatory T (Treg) cells and to abrogate Treg cell-mediated immune suppression via intercellular signaling [24,25]. GITR has also been known to be expressed on activated $CD8^+$ T cells and to act on the induction of tumor-specific $CD8^+$ T cells [26]. In addition, GITR signaling via specific ligands seems to drive $CD8^+$ T cell resistance to Treg cell-mediated inhibition [27]. Currently there is an ongoing clinical trial of a therapeutic anti-human GITR antibody [28]. Thus, GITR targeting is an attractive candidate method for use in HF10 virotherapy as it encourages tumoricidal cytotoxic T lymphocyte (CTL) activity and attenuates immune suppression.

In this study, we examined the anti-tumor effects of i.t. treatment of established murine tumors with HF10 in combination with the GITR-specific agonistic monoclonal antibody (mAb) DTA-1. Our results show that the combination therapy inhibited tumor growth at the contralateral as well as the injected tumor sites by promoting the accumulation of tumor-specific $CD8^+$ T cells followed by DTA-1-mediated depletion of $CD4^+$ $Foxp3^+$ Treg cells. Thus, DTA-1 is an extremely effective partner for HF10 in oncolytic virotherapy.

Materials and Methods

Mice

Female BALB/c mice aged 6–8 weeks were obtained from SLC Japan. BALB/c mice deficient in the γ subunit of the FcγRI, FcγRIII and FcεRI receptors (FcRγ KO mice) [29] were purchased from Taconic and bred at the Mie University Institute of Laboratory Animals. Experimental protocols were approved by the Animal Ethics Committee of Mie University, Tsu, Japan (Approval number: 23-8).

Cell lines

CT26 is a colon tumor cell line derived from BALB/c mice [30]. A CT26 cell line transfected with the gene encoding the human cancer/testis antigen NY-ESO-1 (CT26/NY-ESO-1) was established as described previously [31]. CMS5a is a 3-methyl cholanthrene-induced fibrosarcoma cell line derived from BALB/c mice [32]. A CMS5a cell line transfected with the gene encoding GITR was established by retrovirus-mediated gene transfer. The retrovirus containing the murine GITR gene was purchased from Takara Bio Inc.

CT26/NY-ESO-1 and CMS5a cells were inoculated subcutaneously (s.c.) into the hind flanks of mice (1×10^6 cells/mouse and 2×10^5 cells/mouse, respectively). HF10 or the vehicle was administered i.t. (1×10^7 PFU/mouse) at 7, 8, and 9 days after tumor inoculation. DTA-1 was administered i.t. (10 μg/mouse) at 9 days after tumor inoculation. For the combination therapy, 10 μg of DTA-1 were mixed with the HF10 virus and administered to the mice at 9 days after tumor inoculation.

Antibodies

Fluorescein isothiocyanate (FITC)-conjugated and/or phycoerythrin (PE)-conjugated anti-mouse CD4 (RM4-5; eBioscience, Inc), anti-mouse CD8α mAb (53-6.7; BD Bioscience), anti-mouse/rat Foxp3 mAb (FJK-16s; eBioscience, Inc), anti-mouse IFN-γ mAb (XMG1.2; eBioscience, Inc), anti-mouse F4/80 mAb (BM8; BioLegend), and anti-rat IgG2b monoclonal antibodies (mAbs) (MRG2b-85; BioLegend) as well as a FITC-conjugated rabbit anti-HSV-1 polyclonal antibody (Dako) were used in flow cytometric analysis and immunohistochemstry. An anti-mouse CD16/CD32 mAb (93; eBioscience, Inc) was used for Fc-blocking in all experiments. For *in vivo* administration, anti-mouse GITR mAb (DTA-1, rat IgG2b) and anti-mouse CD8α mAb were purified by protein G affinity column chromatography of ascites from BALB/c nude mice intraperitoneally inoculated with a 53-6.7 hybridoma. Purifed rat serum IgG (Sigma) was used as the control antibody for all experiments with DTA-1. The Fab portion of DTA-1 was prepared by using a Pierce Fab Preparation Kit (Thermo Fisher Scientific) according to the manufacturer's instructions.

Cell preparations

To collect tumor-infiltrating lymphocytes (TILs), a gentleMACS dissociator (Miltenyi Biotec K.K.) was used according to the manufacturer's instructions with some modifications. Briefly, a CT26/NY-ESO-1 tumor cut into small pieces was incubated in 4.5 mL of RPMI-1640 medium supplemented with 1 mg/mL collagenase IA (Sigma) for 40 min at 37°C and then dissociated into single cells using the gentleMACS dissociator. DNase I was not used. The obtained cells were passed through a cell strainer (70 μm) to remove tissue aggregates. After washing 3 times with PBS containing 0.1% BSA, the TILs were evaluated by flow cytometric analysis for intracellular IFN-γ as described below. When DTA-1-binding TIL populations were studied, collagenase I was not used so as to avoid the dissociation of DTA-1 bound to cells.

To investigate DTA-1-mediated generation of tumor-specific $CD8^+$ T cells, DTA-1 was injected i.t. into day 9 CT26/NY-ESO-1 tumors at three doses (0.5, 2, or 10 μg). Tumor-regressed mice were selected from each DTA-1-treated group at 2 weeks after DTA-1 treatment, and the splenocytes from each group were pooled and incubated in RPMI-1640 medium supplemented with 10% fetal calf serum (FCS) and 10 μg/mL of control peptide (9 m: QYIHSANVL) [32], CT26-specific AH-1 peptide (SPSYVYHQF) [33] or NY-ESO-1_{81-88} peptide (RGPESRLL) [34] (all from MBL) for 5 hrs. The obtained cells were analyzed by flow cytometry to determine levels of intracellular IFN-γ.

Splenocytes from CT26/NY-ESO-1-bearing mice obtained at 5 days after i.t. treatment with both HF10 (days 7, 8 and 9) and DTA-1 (day 9) were cultured with CT26-specific AH-1 peptide (10 μg/mL) or HF10-infected CMS5a tumor cells [precultured with HF10 (MOI 1) for 12 hrs and irradiated with 50 Gy] at a ratio of 5 splenocytes to 1 HF10-infected CMS5a cell for 5 hrs. The obtained cells were then evaluated for intracellular IFN-γ as described below.

Flow cytometric analysis of mAb-stained cells

To confirm GITR expression on CMS5a/GITR cells, CMS5a/GITR cells were incubated with DTA-1 ($<2\times10^6$ cells/μg in PBS supplemented with 0.2% BSA) for 15 min at 4°C. After washing 3 times with PBS containing 0.1% BSA, the cells were further treated with FITC-conjugated anti-rat IgG (H + L) Ab (Caltag Lab.) ($<2\times10^6$ cells/μg) for 15 min at 4°C. For staining of intracellular IFN-γ in cultured splenic $CD8^+$ T cells, GolgiPlug (BD Bioscience) protein transport inhibitor was added for the last 4 hrs of the incubation. The obtained cells were permeabilized using a Cytofix/Cytoperm Kit (BD Bioscience) and stained with a CD8α-specific mAb for 15 min at 4°C and followed by an IFN-γ-specific mAb for 15 min at 4°C ($<2\times10^6$ cells/μg). For Foxp3-CD4 double labeling of TILs, TILs were first stained with a CD4-

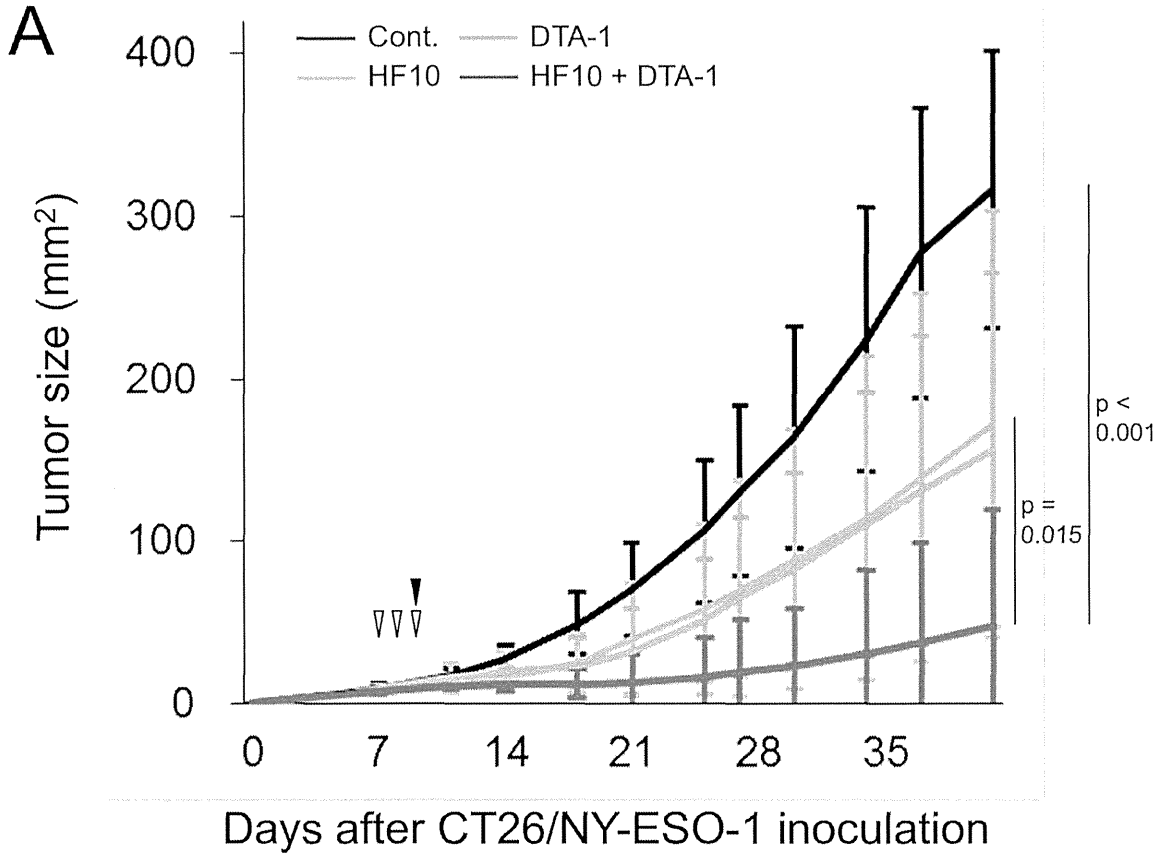
A
Cont.
DTA-1
HF10
HF10 + DTA-1
Tumor size (mm2)
400
300
200
100
0
0
7
14
21
28
35
p < 0.001
p = 0.015
Days after CT26/NY-ESO-1 inoculation

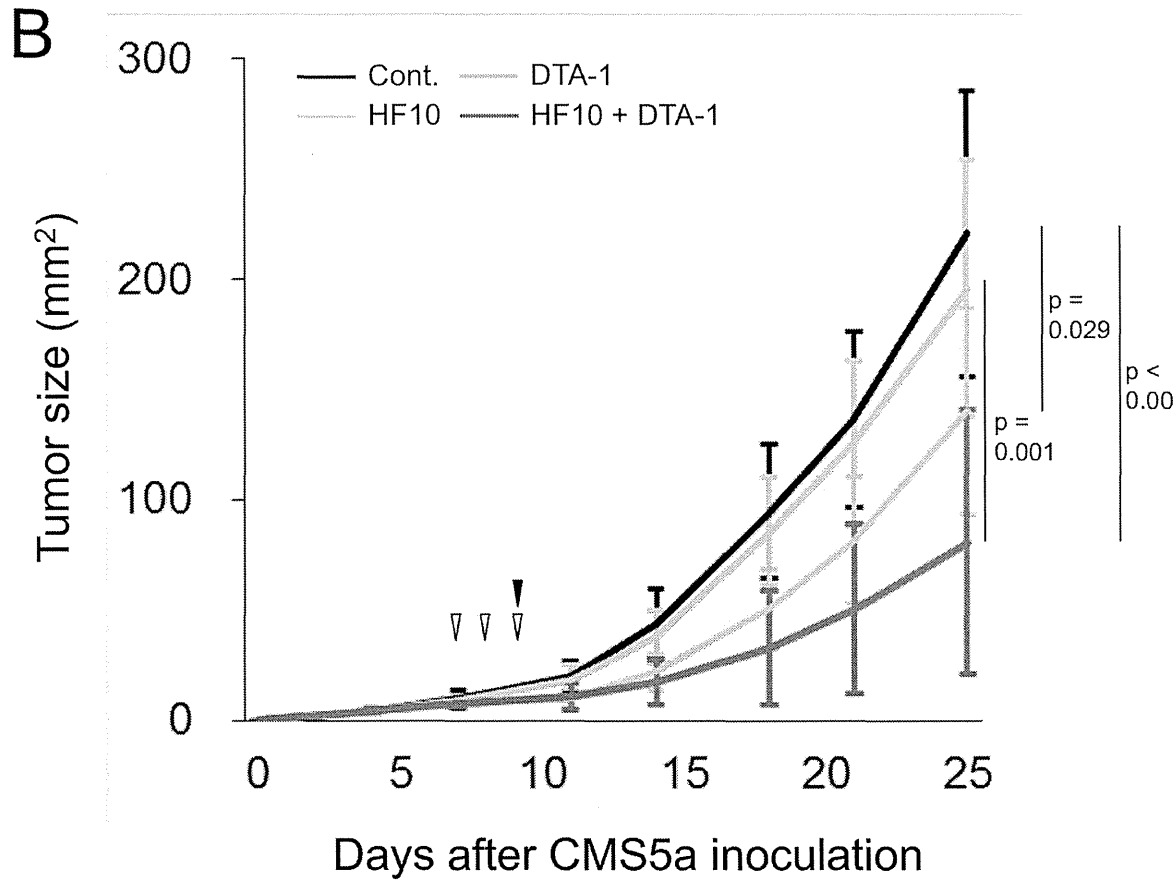
B
Cont.
DTA-1
HF10
HF10 + DTA-1
Tumor size (mm2)
300
200
100
0
0
5
10
15
20
25
p = 0.029
p < 0.001
p = 0.001
Days after CMS5a inoculation

Figure 1. Tumor growth following intratumoral administration of HF10 with/without DTA-1. Growth (mm^2) of subcutaneously inoculated CT26/NY-ESO-1 (A) or CMS5a cells (B) following i.t. treatment with HF10 (open triangles) and/or DTA-1 (closed triangles) on indicated days. Purified rat IgG was used as a control for DTA-1. Data shown in Fig. 1 are representative of four independent experiments. By the Kruskal-Wallis ANOVA test, the CT26/NY-ESO-1 growth inhibition by combined treatment with HF10 and DTA-1 was significantly different from the HF10-treated or untreated control at day 42. CMS5a growth inhibition by the HF10 and DTA-1 combination was significantly different from the DTA-1-treated or untreated control at day 25. CMS5a growth inhibition was also significantly different in the HF10-treated group compared with the untreated control.
doi:10.1371/journal.pone.0104669.g001

specific mAb [15 min, 4°C ($<2\times10^6$ cells/μg)], then fixed and permeabilized using a Foxp3 staining kit (eBioscience, Inc.), and then treated with a Foxp3-specific mAb [30 min, 4°C ($<1\times10^6$ cells/μg)]. The labeled cells were then analyzed by flow cytometry (FACSCanto II: BD Bioscience) with FlowJo software (Tomy Digital Biology).

Immunohistochemistry

Frozen CT26/NY-ESO-1 tumor specimens embedded in O.C.T compound (Sakura Finetechnical) were sectioned at a thickness of 3 μm, air dried for 2 hrs, fixed with cold acetone for 15 min, and then processed for immunohistochemistry. After washing 3 times with PBS, the slides were incubated at 4°C in blocking solution [PBS supplemented with 1% BSA, 5% Blocking One Histo (Nacalai Tesque, Inc.)] and 0.2 μg/mL anti-mouse CD16/CD32 mAb for 30 min. The tumor sections on the slides were then dual-labeled with PE-conjugated mAb and FITC-conjugated mAb diluted with PBS supplemented with 1% BSA and 5% Blocking One Histo for 1 hr at room temperature (r.t.) in a humidified chamber. After washing 3 times with PBS supplemented with 0.02% Tween-20, the slides were mounted in ProLong Gold antifade reagent with DAPI (Invitrogen, Life Technologies, Inc.), and evaluated by fluorescence microscopy (BX53F; Olympus Co. Ltd.; Tokyo, Japan). The photographs from PE-, FITC-, and DAPI-stained tissue sections were merged and background fluorescence was deleted using Photoshop elements software (Adobe Systems Software Ltd.).

For hematoxylin and eosin (HE) staining, slides with acetone-fixed tissue sections were washed 3 times with PBS and incubated at r.t. in hematoxylin solution (New Hematoxylin Sol.: Muto Pure Chemicals Co., Ltd.) for 5 min. After washing with tap water, the cytoplasm was stained with eosin (r.t. for 2 min.; Pure Eosin Sol.: Muto Pure Chemicals). Samples were then dehydrated 3 times with xylene, and the slides were mounted with Malinol (Muto Pure Chemicals) and evaluated by microscopy.

Antibody-dependent cellular cytotoxicity (ADCC) assay

RAW264.7 cells were activated with 20 ng/mL murine IFN-γ for 24 hrs in 24-well plates, after which the cells were gently washed with RPMI-1640 and the dish-adherent RAW264.7 cells were used as effectors in the ADCC assay. CMS5a or CMS5a/GITR cells were labeled with 2.5 μM carboxyfluoresceine diacetate succinimidyl ester (CFSE) at 37°C for 6 min to be used as targets in the ADCC assay. After washing 3 times with RPMI-1640 supplemented with 10% FCS, CFSE-labeled CMS5a or CMS5a/GITR cells were plated at various effector-to-target ratios with rat IgG or DTA-1 (2 μg/mL), incubated for 12 hrs, and analyzed by flow cytometry. For each sample, 20,000 non-CFSE labeled cells were collected, and the absolute number of CFSE-labeled surviving cells was counted. The survival percentage was calculated as the mean number of each of the three wells as follows: [(absolute number of surviving CFSE-labeled cells in control rat IgG-containing medium)−(absolute number of surviving CFSE-labeled cells in DTA-1-containing medium)]×100/(absolute number of surviving CFSE-labeled cells in control rat IgG-containing medium).

Statistical analysis

The Mann-Whitney U test was used to compare data from two groups. When equality of variance was proven by Levine's test, data comparison between 2 groups was evaluated by Student's *t*-test. The Kruskal-Wallis ANOVA test was used to compare data from four groups. *p*-values below 0.05 were considered statistically significant. Calculations were performed using SPSS Statistics v21.0 software (IBM).

Results

Effective inhibition of tumor growth by local treatment of HF10 combined with DTA-1

Since the therapeutic efficacy of the adjuvants included in immune-targeting Abs has been widely shown in the treatment of cancer, we hypothesized that the use of DTA-1, as an enhancer of tumor-specific $CD8^+$ T cell responses [26,27] in HF10 virotherapy might produce a satisfactory treatment outcome. To investigate this hypothesis, we used human NY-ESO-1 gene-transfected CT26 tumor cells (CT26/NY-ESO-1) for *in vitro* and *in vivo* studies as an H-$2D^d$-restricted murine CTL epitope of NY-ESO-1 had been identified in our laboratory [31]. Subcutaneously inoculated CT26/NY-ESO-1 tumors were treated by i.t. administration of HF10 with or without DTA-1 (Fig. 1A). Groups treated with either HF10 or DTA-1 showed weak suppression of tumor growth compared with the untreated group (control), and 2 out of 13 mice (15.4%) or 3 out of 19 mice (15.8%) showed

Table 1. Increase in the number of tumor-regressed mice by HF10 therapy combined with DTA-1.

Treatment	Number of complete tumor-regressed mice*/Number of treated mice (%)	
	CT26/NY-ESO-1	CMS5a
Cont. IgG	0/10 (0.0%)	0/13 (0.0%)
DTA-1	2/13 (15.4%)	0/13 (0.0%)
HF10	3/19 (15.8%)	0/13 (0.0%)
HF10+DTA-1	12/20 (60.0%)	3/13 (23.1%)

* Number of complete tumor-regressed mice was counted at 42 or 25 days after subcutaneous inoculation of CT26/NY-ESO-1 or CMS5a tumor cells, respectively.
doi:10.1371/journal.pone.0104669.t001

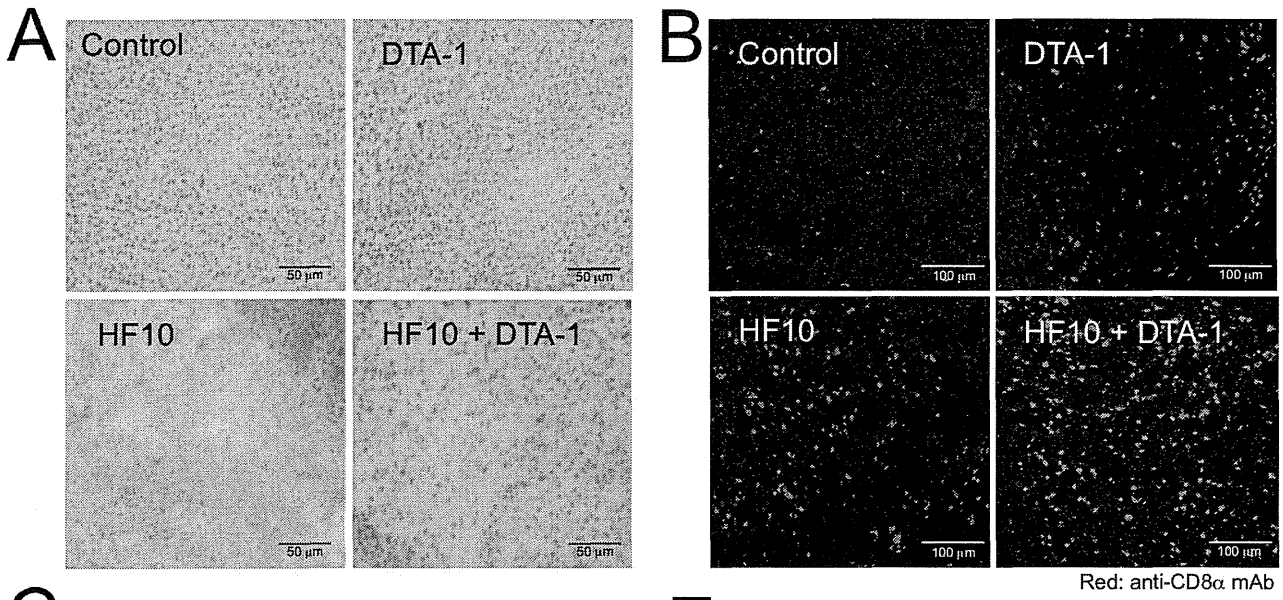
A
Control
DTA-1
HF10
HF10 + DTA-1
50 μm
B
Control
DTA-1
HF10
HF10 + DTA-1
100 μm
Red: anti-CD8α mAb

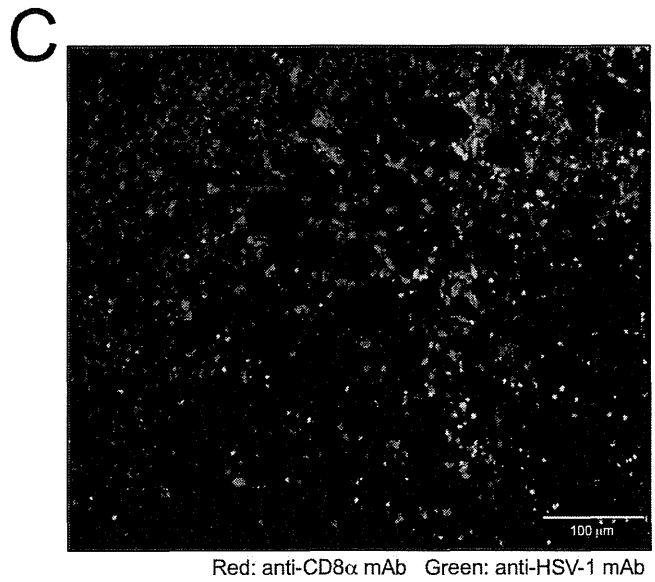
C
100 μm
Red: anti-CD8α mAb Green: anti-HSV-1 mAb

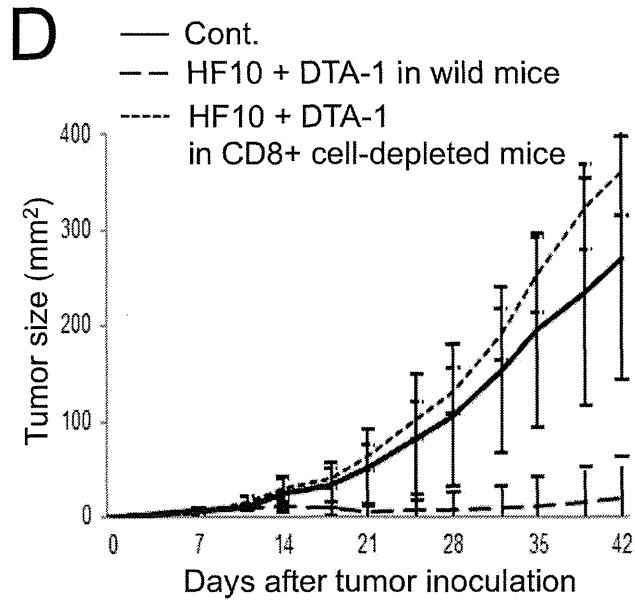
D
Cont.
HF10 + DTA-1 in wild mice
HF10 + DTA-1
in CD8+ cell-depleted mice
Tumor size (mm2)
400
300
200
100
0
0
7
14
21
28
35
42
Days after tumor inoculation

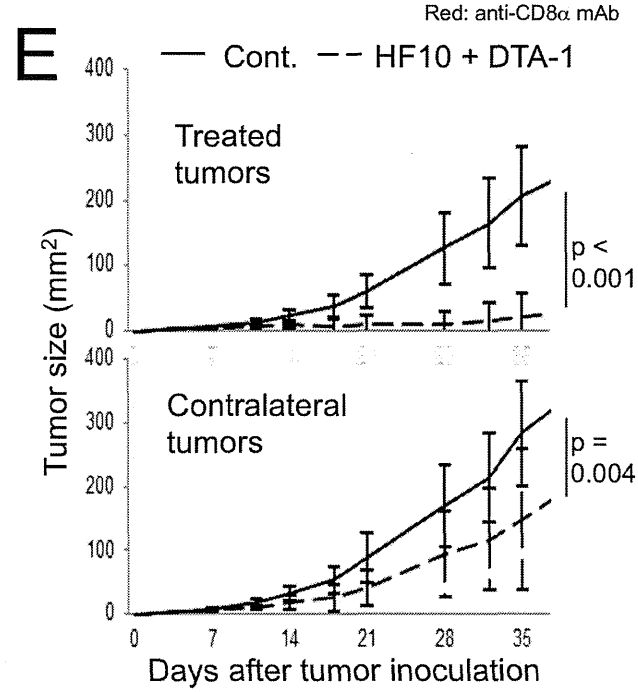
E
Cont.
HF10 + DTA-1
Treated
tumors
p <
0.001
Contralateral
tumors
p =
0.004
Tumor size (mm2)
400
300
200
100
0
0
7
14
21
28
35
Days after tumor inoculation

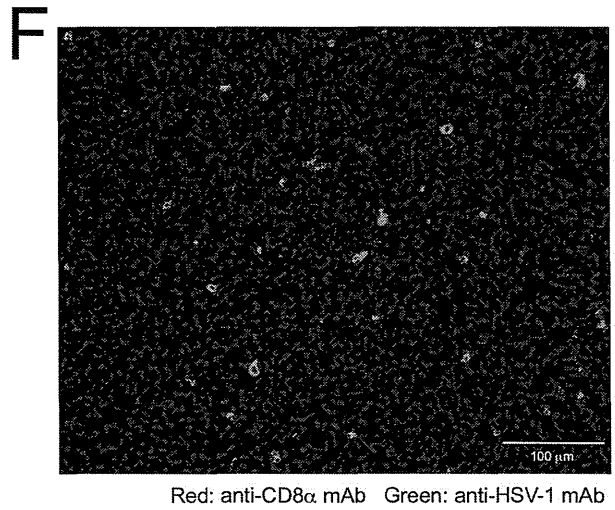
F
100 μm
Red: anti-CD8α mAb Green: anti-HSV-1 mAb

Figure 2. Kinetics of $CD8^+$ T cells after the combination therapy with HF10 and DTA-1. CT26/NY-ESO-1 tumor sections from untreated mice (control) or mice injected i.t. with DTA-1, HF10, or HF10 combined with DTA-1 were stained with hematoxylin and eosin (A), and phycoerythrin (PE)-conjugated anti-CD8α mAb and DAPI (B). (C) Frozen sections of CT26/NY-ESO-1 tumors from mice i.t. injected with HF10 combined with DTA-1 were stained with a PE-anti-CD8α monoclonal antibody, a fluorescein isothiocyanate (FITC)-anti-HSV-1 polyclonal antibody, and DAPI. (D) CT26/NY-ESO-1 growth (mm^2) in both i.t. HF10- and DTA-1-treated control or $CD8^+$ cell-depleted mice was measured. Seven mice per group were used. (E) Bilateral CT26/NY-ESO-1-bearing mice were treated with a combination of HF10 and DTA-1 in the tumors on the right flanks. Subsequent tumor growth (mm^2) of the treated right and contralateral left sites was measured. Tumor growth in untreated mice was measured and used as a control. Fourteen mice per group were used. By the Kruskal-Wallis ANOVA test, CT26/NY-ESO-1 growth inhibition by the combined HF10 and DTA-1 treatment in contralateral as well as treated sites was significantly different from the untreated control group. (F) CT26/NY-ESO-1 tumors from one side of bilateral tumor-bearing mice were treated i.t. with HF10 combined with DTA-1. Frozen sections of contralateral CT26/NY-ESO-1 tumors were stained with a PE-anti-CD8α monoclonal antibody, a fluorescein isothiocyanate (FITC)-anti-HSV-1 polyclonal antibody, and DAPI.
doi:10.1371/journal.pone.0104669.g002

complete tumor regression at 42 days after tumor inoculation, respectively (Table 1). In contrast, all mice in the group treated with both HF10 and DTA-1 showed statistically significant attenuation of tumor growth compared with the control group [$p<0.001$, Fig. 1A; complete tumor regression rate at 42 days: 60.0% (12 to 20 mice); Table 1]. In addition, CMS5a tumor growth in the group treated with both HF10 and DTA-1 was also suppressed significantly compared with the control or DTA-1-treated groups (Fig. 1B and Table 1).

We observed CT26/NY-ESO-1-regressed mice in another experiment for 2 months after HF10 and DTA-1 treatment. Tumor recurrence could not be seen in the tumor-regressed mice. In addition, these mice exhibited the resistance in tumor re-challenging.

$CD8^+$ T cells act as tumoricidal effectors in the combination therapy of HF10 with DTA-1

Intratumoral injection of HF10 resulted in the collapse of tumor structure with a decrease in the nuclear density of tumor cells, as shown at 7 days after the last HF10 treatment in both the group treated with HF10 and that treated with HF10 and DTA-1 (Fig. 2A). Tumor-infiltrating $CD8^+$ T cells were shown to be the most frequent population after the administration of HF10 combined with DTA-1 at 3 days after the final treatment (Fig. 2B). Importantly, these cells appeared to accumulate near HF10-infected tumor areas (Fig. 2C and S1A), suggesting that HF10 infection is able to attract $CD8^+$ T cells by leaking virus-associated proteins and tumor antigenic proteins from infected tumor cells and changing the tumor microenvironment after oncolysis. Inhibition of CT26/NY-ESO-1 growth by the combination therapy was completely negated by depleting $CD8^+$ cells by intravenous treatment with a murine CD8α-specific mAb (Fig. 2D), indicating that the tumor-infiltrating $CD8^+$ T cells shown in Figure 2B and 2C include tumoricidal effector populations. In the study using bilateral tumor-bearing mice, tumor growth inhibition by HF10 combined with DTA-1 occurred not only in the treated tumors but also in the contralateral non-treated tumors (Fig. 2E and S1B). In addition, the sections of contralateral tumor showed infiltrating $CD8^+$ T cells without HF10 infection (Fig. 2F and S1C). These results indicate that $CD8^+$ T cells activated in a local tumor site under the influence of HF10 and DTA-1 participate in systemic surveillance and could attack distant tumors without tissue destruction due to HF10 infection.

Augmentation of tumor-specific $CD8^+$ T cell responses by DTA-1 treatment in HF10 therapy

Next, we investigated whether the tumor- or HF10-specific $CD8^+$ T cell response was enhanced in CT26/NY-ESO-1-bearing mice by i.t. treatment with DTA-1 alone or HF10 combined with DTA-1. To detect low proportions of $CD8^+$ T cells with tumor specificity, spleen cells from tumor-regressed mice selected after i.t. treatment with DTA-1 at the indicated doses were stimulated with a CT26-specific AH-1 peptide or an NY-ESO-1 81–88 peptide to expand each population of peptide-specific $CD8^+$ T cells. As shown in Figure 3A, the response of CT26-specific IFN-γ-producing $CD8^+$ T cells was enhanced by DTA-1 in a dose-dependent manner. In addition, $CD8^+$ T cells with NY-ESO-1 specificity were observed when DTA-1 was administered at a high dose (10 μg). In this experiment, we used tumor-regressed mice because we could not enhance the negligible CT26-specific IFN-γ-producing $CD8^+$ T cell responses seen in tumor-bearers in a DTA-1 dose-dependent manner. Although CT26/NY-ESO-1 growth after i.t. treatment with DTA-1 was suppressed compared with the control group, tumor size was not different in each group of DTA-1 (0.5, 2.0, or 10.0 μg/mouse). Furthermore, HF10-specific $CD8^+$ T cells were found in addition to the AH-1-specific population (Fig. 3B left) when splenocytes from both HF10- and DTA-1-treated CT26/NY-ESO-1-bearing mice with HF10-infected CMS5a cells were cultured (Fig. 3B right). These results indicated that i.t. treatment of HF10 and DTA-1 had the capacity to enhance tumor- and HF10-specific $CD8^+$ T cell populations.

Disappearance of tumor-infiltrating $Foxp3^+$ cells after the treatment with DTA-1 in HF10 therapy

We hypothesized that the increase in tumor-specific $CD8^+$ T cell responses after DTA-1 treatment combined with HF10 therapy was involved in the attenuation and/or depletion of immune suppressors including Treg cells. To address this issue, CT26/NY-ESO-1 tumors obtained after DTA-1 treatment with or without HF10 were evaluated by immunohistological staining of tissue sections and flow cytometric analysis of infiltrating lymphocytes using a Foxp3-specific mAb. $Foxp3^+$ cells accumulated abundantly in both untreated and HF10-treated tumors, whereas a vigorous decrease in the number of Treg cells was shown in tumors following treatment with DTA-1 alone or DTA-1 combined with HF10 (Fig. 4A). This result was confirmed by flow cytometric analysis of tumor-infiltrating Treg cells. The frequency of tumoral $CD4^+$ $Foxp3^+$ Treg cells from the HF10- and DTA-1-treated group was decreased significantly compared with that from the untreated (control) group but not from the HF10- or DTA-1-treated mice (Fig. 4B). The decrease in the frequency of $Foxp3^+$ cells in the HF10-treated group (Fig. 4B) is possibly correlated with the decrease in tumor size due to HF10 treatment. This may be attributed to the lack of modulation of the absolute number of $Foxp3^+$ cells in the HF10-treated group unlike in the control group (Fig. 4A). DTA-1 is a rat IgG2b class mAb. By visualizing DTA-1 with the FITC-conjugated anti-rat IgG2b mAb, it was demonstrated that the tumor-infiltrating $CD4^+$ $Foxp3^+$ Treg population bound predominantly with DTA-1 at 6 hrs after i.t. injection (Fig. 4C), in parallel with the disappearance of tumoral Treg cells after treatment with DTA-1. Taken together, these results strongly indicate that DTA-1 was essential to the decrease in the number of $CD4^+$ $Foxp3^+$ cells.

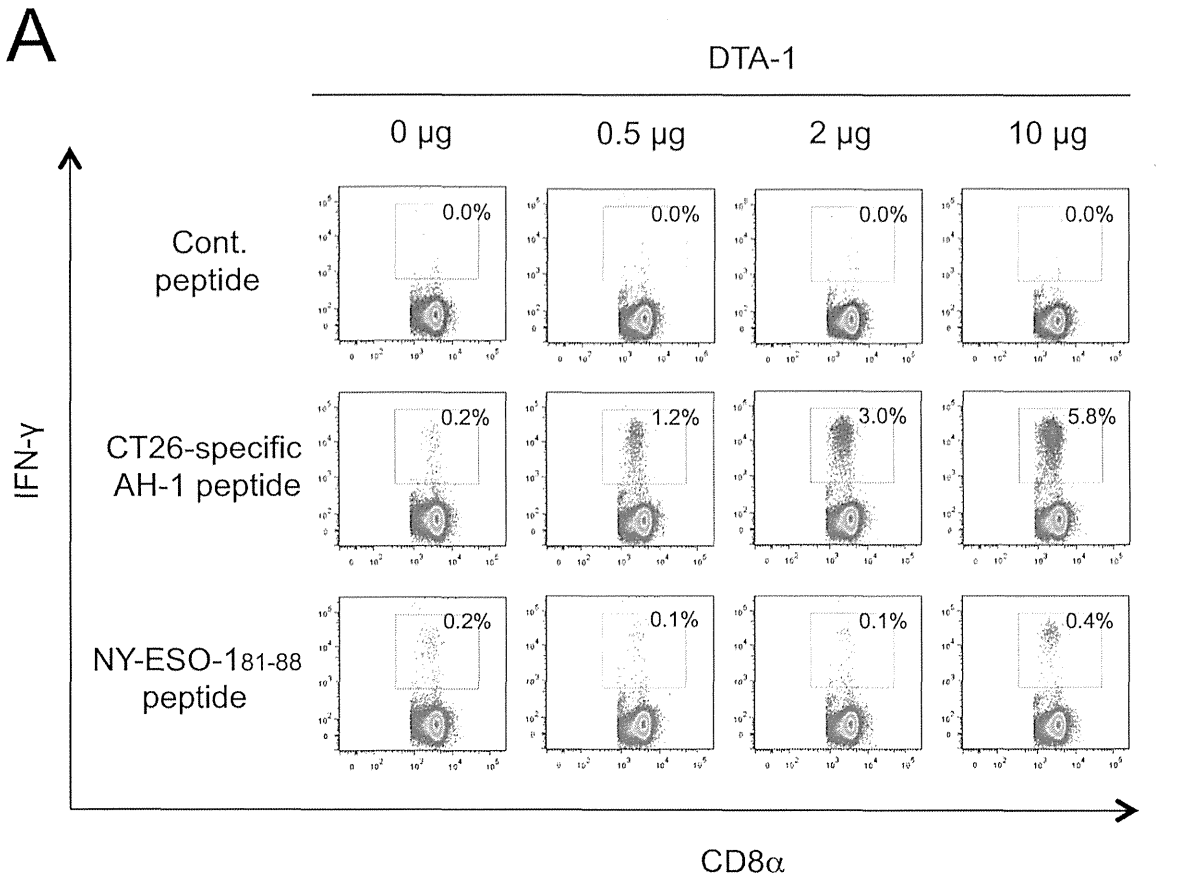

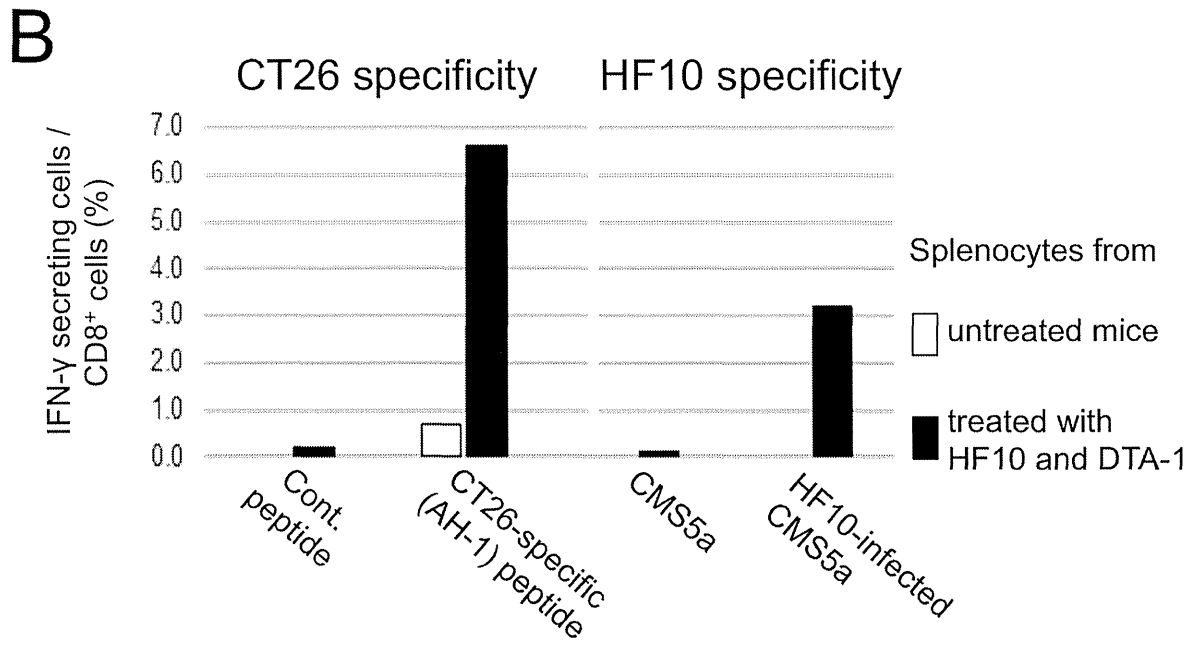

Figure 3. Generation of tumor- and HF10-specific CD8$^+$ T cells by intratumoral treatment of DTA-1 and HF10 combined with DTA-1. (A) CT26- and NY-ESO-1-specific CD8$^+$ T cell responses in CT26/NY-ESO-1-regressed mice by i.t. treatment of DTA-1 at indicated doses were assessed by intracellular staining of IFN-γ in splenocytes cultured with 10 μg/mL of the indicated peptides for 5 hrs. Splenocytes from two mice per group were pooled and assessed. (B) Splenocytes from untreated and both i.t. HF10- and DTA-1-treated CT26/NY-ESO-1-bearing mice were obtained at 5 days after final treatment, and cultured with AH-1 peptide (10 μg/mL) or HF10-infected CMS5a tumor cells for 5 hrs. Splenocytes from ten mice per group were pooled and assessed. The obtained cells were immunohistologically stained for intracellular IFN-γ. The 9 m peptide and uninfected CMS5a cells were used as controls.
doi:10.1371/journal.pone.0104669.g003

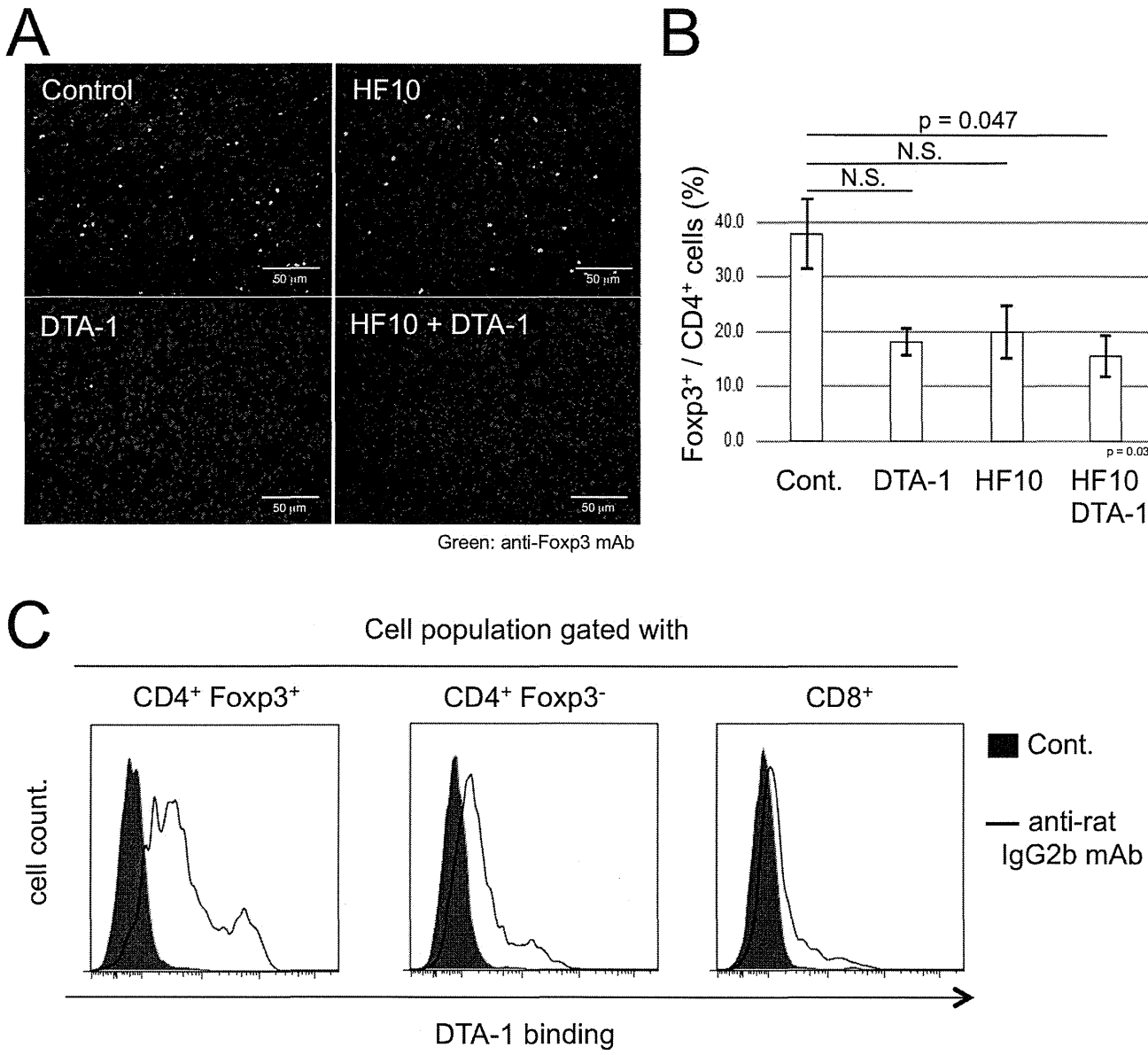

Figure 4. Disappearance of DTA-1-conjugated tumor-infiltrating CD4$^+$ Foxp3$^+$ cells after combined i.t. treatment with HF10 and DTA-1. (A) CT26/NY-ESO-1 tumor sections form untreated group (control) or group from mice injected i.t. with DTA-1, HF10, or HF10 combined with DTA-1 were stained with FITC-anti-Foxp3 mAb and DAPI. (B) The frequency of tumor-infiltrating CD4$^+$ Foxp3$^+$ Treg cells from mice injected i.t. with HF10, DTA-1, or HF10 combined with DTA-1 at 12 days after CT26/NY-ESO-1 inoculation was assessed by flow cytometry. Data from 4 individual experiments were analyzed statistically. Kruskal-Wallis ANOVA test was used to compare data from the 4 groups. The decrease in the frequency of tumoral CD4$^+$ Foxp3$^+$ Treg cells in the HF10 and DTA-1 combined treatment group was significantly different from untreated control, but not from the HF10- or DTA-1-treated group (N.S: Not significant). (C) At 6 hrs after DTA-1 injection into day 9 CT26/NY-ESO-1 tumors, tumor-infiltrating cells collected under collagenase-free conditions were analyzed by flow cytometry after staining with FITC-labeled anti-rat IgG2b mAb to detect DTA-1-bound cells.
doi:10.1371/journal.pone.0104669.g004

Depletion of tumor-infiltrating Treg cells by DTA-1-mediated cellular cytotoxicity

Fluorescent immunohistological studies using double labeling with anti-rat IgG2b mAb (for DTA-1) and F4/80- (for macrophages) or Foxp3- (for Tregs) specific mAbs were performed to determine the mechanisms of DTA-1-dependent depletion of CT26/NY-ESO-1 tumor-infiltrating Treg cells. At 6 hrs after DTA-1 treatment, Foxp3$^+$ cells clustered at the DTA-1-stained peritumor sites, whereas Foxp3$^+$ cells did not accumulate in the control rat IgG-treated case (Fig. 5A and S2A). Images of red fluorescence from DTA-1 or the control rat IgG merged with the green fluorescence from F4/80$^+$ macrophages in nearby tumor stroma (Fig. 5B; C1, D1, and S2B) indicated that DTA-1 and rat IgG bound with macrophage-expressing FcRs. In addition, a large number of cells visualized in lymphocyte-like formation by staining with anti-rat IgG2b mAb were positive for Foxp3 (Fig. 5B; D2, D3; Fig. S3A and B) and were in contact with macrophages in various areas of DTA-1–treated tumors (Fig. 5B; D2; Fig. S3A). These results strongly support the hypothesis that DTA-1

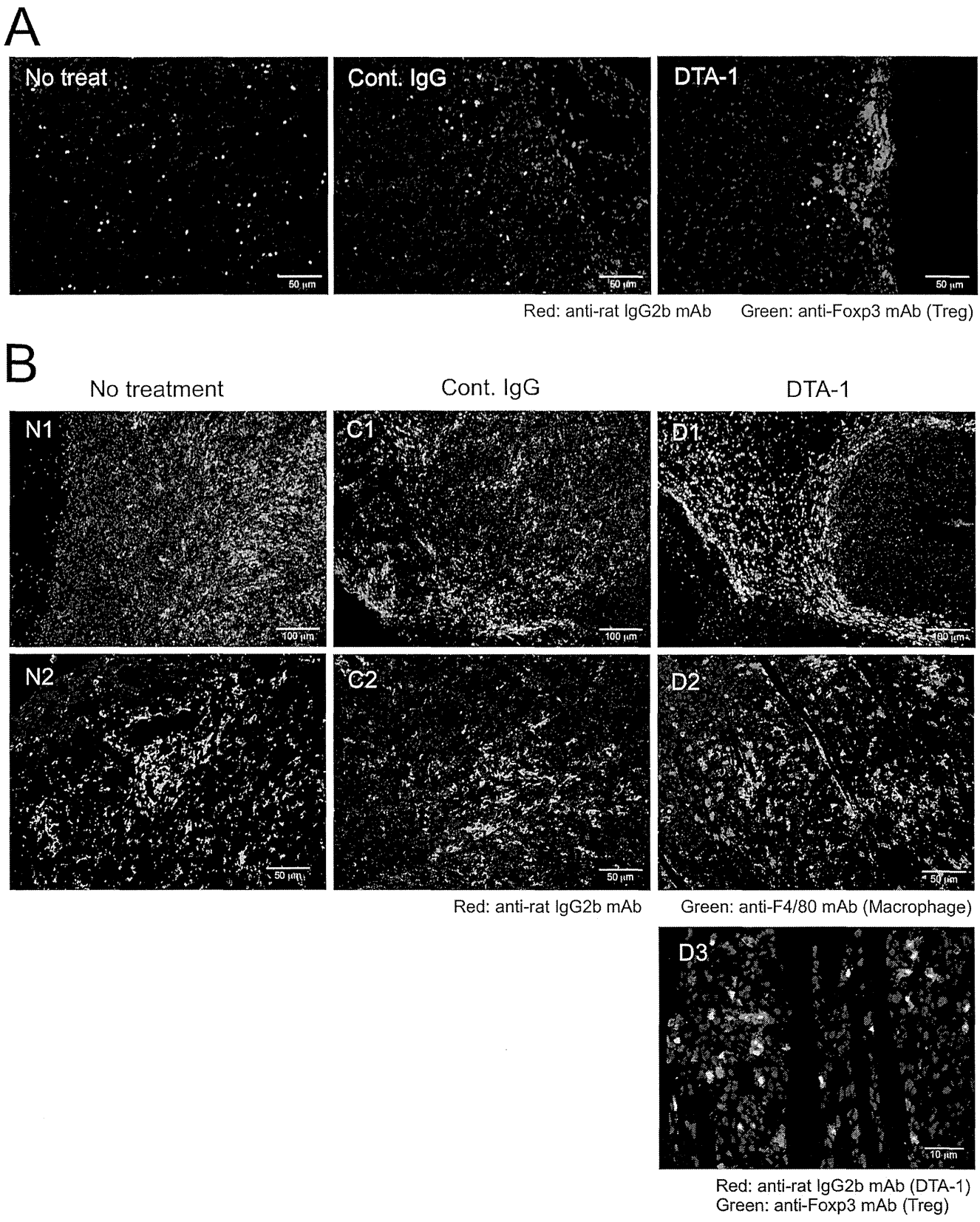

Figure 5. Kinetics of Foxp3$^+$ Treg cells and F4/80$^+$ macrophages in DTA-1-treated tumors. Frozen sections of CT26/NY-ESO-1 tumors obtained at 6 hrs after DTA-1 i.t. injection were stained with FITC-conjugated anti-Foxp3 mAb, PE-conjugated anti-rat IgG2b mAbs and DAPI (A and B: D3), or FITC-anti-F4/80 mAb, PE-anti-rat IgG2b mAb, and DAPI (B: D1 and D2). Sections from untreated and control rat IgG-treated tumors were used as controls (A and B: N1, N2, C1, C2). Representative photos from three experiments are shown.
doi:10.1371/journal.pone.0104669.g005

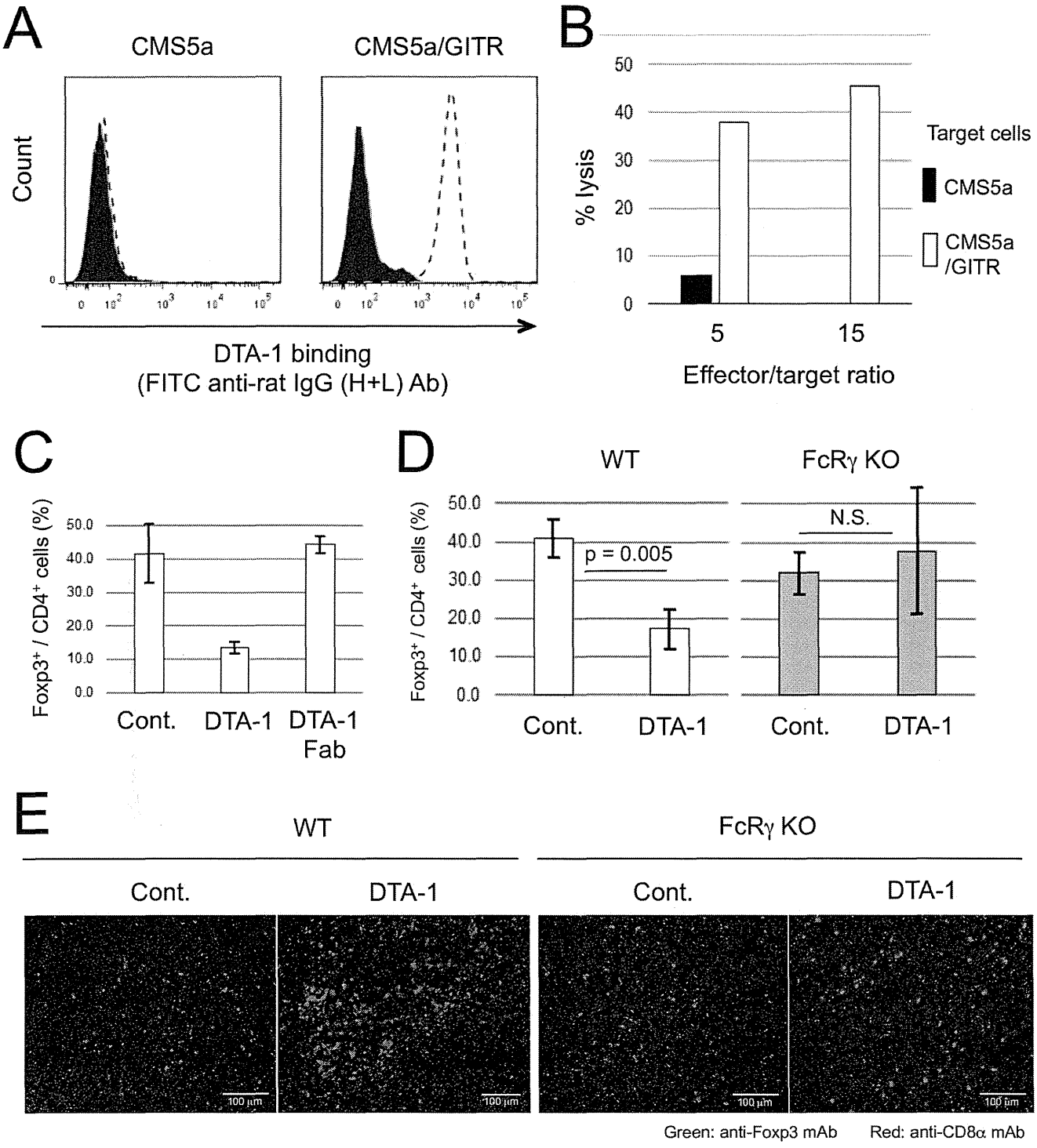

Figure 6. DTA-1-mediated depletion of tumor-infiltrating CD4$^+$ Foxp3$^+$ Treg cells by ADCC. (A) DTA-1- (dotted line) or isotype control (solid line)-treated CMS5a and murine GITR gene-transfected CMS5a (CMS5a/GITR) cells were stained with a FITC-conjugated anti-rat IgG (H+L) antibody and analyzed by flow cytometry. (B) CFSE-labeled CMS5a and CMS5a/GITR cells were used as targets. The mixture of IFN-γ-activated RAW264.7 cells (effector cells) and target cells were incubated for 12 hrs with control IgG or DTA-1 at effector/target ratios of 5 and 15. (C) Frequency of Foxp3$^+$ cells in tumor-infiltrating CD4$^+$ cell population at 3 days after i.t. DTA-1 or Fc-digested DTA-1 (DTA-1 Fab) treatment was measured by flow cytometric analysis. (D) Frequency of Foxp3$^+$ cells in tumor-infiltrating CD4$^+$ cell population at 3 days after DTA-1 i.t. treatment in wild-type or FcRγ KO mice was measured by flow cytometric analysis. By Student's t-test, the decrease in the frequency of Foxp3$^+$ cells in DTA-1-treated CT26/NY-ESO-1 tumors of wild type mice, but not FcRγ KO mice (N.S.: Not significant), was significantly different from untreated control group. (E) Frozen sections of CT26/NY-ESO-1 tumors obtained at 3 days after DTA-1 i.t. treatment in wild type and FcRγ KO mice were stained with FITC-anti-Foxp3 and PE-anti-CD8α mAbs, and DAPI.

doi:10.1371/journal.pone.0104669.g006

participates in GITR$^+$ Foxp3$^+$ Treg depletion by ADCC at the treated tumor sites.

To examine whether DTA-1 can mediate ADCC in a murine system, we performed an *in vitro* ADCC assay using IFN-γ-activated RAW264.7 macrophage cells as an effector and murine GITR gene-transfected CMS5a (CMS5a/GITR) cells (Fig. 6A) as a target. CMS5a/GITR cells were lysed in the presence of DTA-1 in a GITR-specific manner (Fig. 6B). We further investigated *in vivo* the ADCC effects of DTA-1 using Fc portion-digested DTA-1 (DTA-1 Fab) and FcRγ KO mice. Depletion of CD4$^+$ Foxp3$^+$ Treg cells in CT26/NY-ESO-1 tumors was not observed following i.t. DTA-1 Fab treatment (Fig. 6C). In addition, no significant decreases in the number of CD4$^+$ Foxp3$^+$ Treg cells and accumulation of CD8$^+$ T cells were detected by DTA-1 treatment in FcRγ KO mice, unlike the results from wild-type mice (Fig. 6D, 6E, and S4). These results clearly indicated the direct participation of DTA-1 in Treg cell depletion by ADCC.

Taken together, these results show that HF10 virotherapy combined with DTA-1 elicits a powerful therapeutic effect against tumors via the accumulation of CD8$^+$ T cells, after tumor destruction by HF10 and the enhancement of tumor- and virus-specific CD8$^+$ T cell responses directly or indirectly by depletion of immune-suppressive Treg cells at tumor sites by DTA-1.

Discussion

Many studies involving oncolytic virus combined with systemic administration of cytotoxic agents have shown promising results in animal models. However, almost all of the studies have avoided the important issue of lymphocyte suppression caused by steroids as an antiemetic, implying the clinical inapplicability of such cytotoxic agents. Tumor therapy promises an era of safety in using noninvasive immunomodulatory agents including PD-1-, CTLA-4- and GITR-specific mAbs. Unfortunately, all of them have produced slight immune-related slight adverse events such as diarrhea, rashes or pruritis [35–38]. In addition, systemic administration of immunomodulators can elicit serious autoimmune diseases. A study from another group has shown that in a murine model, treatment with 50 μg/mouse DTA-1 induces antitumor activity and weak autoimmune reactions [39]. In this study, we also demonstrated that HF10 virotherapy combined with a GITR-targeting mAb in local tumor sites at more clinical appropriate lower and safer doses, elicits tumor lysis by augmented systemic tumor-specific CD8$^+$ T cell activity with negligible toxicity. Therefore, local treatment of immunomodulators is a promising method for the future treatment of tumors.

The use of blocking Abs for suppressing immune signals has shown clinical benefits in the treatment of solid tumors [40–42]. Both PD-1 and CTLA-4, which are expressed on activated T cell surfaces, inhibit tumoricidal effector T cell responses by engagement via specific ligands that are expressed on various tumor cells [23]. However, high densities of tumor-infiltrating CD4$^+$ CD25$^+$ Foxp3$^+$ Treg cells have been correlated with poor survival [43–45]. Treg cells express both PD-1 and CTLA-4 in the steady state without activation. PD-1 and CTLA-4 signals result in Treg induction and maintenance, and subsequent outbreak of autoimmune diseases [46]. Interestingly, it has been reported that an anti-CTLA-4 antibody augments tumoricidal effector T cells by downregulation of Treg cell functions, including ADCC-mediated depletion of Treg cells [47], which is similar to our GITR-targeting results. These reports indicate that the blockade of immune checkpoint molecules involves the activation of tumoricidal effector T cells by preventing interactions with specific ligands on tumor cells and inhibiting Treg cell functions.

The expression of GITR has been observed on CD4$^+$ CD25$^+$ Treg cells at relatively high levels [24,25], which is consistent with our results. In addition, the GITR-GITRL interaction has been known to attenuate Treg cell function via the loss of Foxp3 expression as well as enhance tumor-specific effector CD4$^+$ and CD8$^+$ T cell functions [27,39,48,49]. In this study, we demonstrated the use of DTA-1 as a depletion antibody because Fc-digested DTA-1 and intact DTA-1 in FcRγ KO mice did not participate in the downregulation of Foxp3 expression. After i.t. DTA-1 injection, macrophages appeared to attract DTA-1-conjugated Treg cells via their FcR and migrate to peritumor sites, as shown in Fig. 5, and the results suggest that the peritumoral stroma is a crucial place for ADCC triggering. Since CCL22 secreted by macrophages is known to be a chemoattractant for Treg cells [43,50], such chemokines might participate in DTA-1-mediated Treg cell depletion. Further studies are necessary to elucidate the molecular mechanisms of tumoral ADCC.

As indicated in Fig. 4C, a small proportion of tumor-infiltrating CD8$^+$ T cells bound with i.t. treated DTA-1. In addition, DTA-1 enhanced tumor-specific CD8$^+$ T cell responses in a dose-dependent manner in tumor-regressed mice as shown in Fig. 3. These results suggest that DTA-1 acts as a direct activator of CD8$^+$ T cells, although we could not rule out the possibility that tumor-specific CD8$^+$ T cell responses were increased by DTA-1 dose-dependent depletion of immune suppressive Treg cells. Indeed, it has been reported that the function and activity of CTLs are augmented by the signals through GITR [26,48,51]. In this study, HF10-specific CD8$^+$ T cells were detected after both HF10 and DTA-1 injections, concomitant with vigorous tumor-specific CTL responses. La et al. have reported that DTA-1 elicits immediately explosive HSV-1-specific CD8$^+$ CTL and CD4$^+$ Th responses in HSV-1-infected mice [52]. In addition, we found in this study that DTA-1 was detected in tumor-draining lymph nodes soon after i.t. injection (Fig. S5), suggesting the relationship between DTA-1 and quick generation of tumor-specific CTLs. Thus, it is likely that HF10-specific CTL responses induced by DTA-1 change the tumor microenvironment to facilitate the expansion of CTLs in tumor-draining lymph nodes.

In conclusion, local HF10 therapy combined with DTA-1 should be suitable for the treatment of cancer patients without crucial side effects. The benefits of the combined treatment regimen include the vigorous expansion of tumoricidal CTLs associated with the early HF10-specific CTL responses, inhibition of tumor formation by HF10 infection, direct expansion of CD8$^+$ T cells by DTA-1, and negation of immune suppressive Treg cell activities by DTA-1-mediated ADCC and/or DTA-1 signaling.

Supporting Information

Figure S1 Systemic surveillance of tumoricidal CTLs after HF10 combination therapy with DTA-1 at local tumor sites. (A) The images of red (PE), green (FITC), and blue (DAPI) fluorescence that were merged to produce Fig. 2C. (B) Bilateral CT26/NY-ESO-1-bearing mice were treated i.t. with a combination of HF10 and DTA-1 in tumors on the right flanks of mice. Tumor growth in the treated right and contralateral left sites was measured. Photos show representative mice at 25 days after CT26/NY-ESO-1 inoculation from the control and dual HF10- and DTA-1-treated groups. (C) The three images of red (PE), green (FITC), and blue (DAPI) fluorescence that were merged to produce Fig. 2F.
(TIF)

Figure S2 The three fluorescence components of the merged images of Fig. 5A and Fig. 5B (N1, C1, and D1).

Three separate images of red (PE), green (FITC), and blue (DAPI) fluorescence that were merged to produce Fig. 5A (A) and N1, C1, and D1 of Fig. 5B (B).
(TIF)

Figure S3 The three fluorescence components of the merged images of N2, C2, D2, and D3 in Fig. 5B. The three separate images of red (PE), green (FITC), and blue (DAPI) fluorescence that were merged to produce N2, C2, D2, and D3 images in Fig. 5B.
(TIF)

Figure S4 The three fluorescence components of the merged images in Fig. 6E. The three separate images of red (PE), green (FITC), and blue (DAPI) fluorescence that were merged to produce Fig. 6E.
(TIF)

Figure S5 Drafting of i.t. treated DTA-1 into tumor-draining lymph nodes. Frozen sections of tumor-draining lymph nodes obtained at 6 hrs after intratumoral DTA-1 or DTA-1 Fab treatment were stained with a FITC-conjugated anti-rat IgG2b antibody, a phycoerythrin (PE)-conjugated anti-F4/80 antibody, and DAPI.
(TIF)

Acknowledgments

We thank Drs. N. Harada, Y. Miyahara, T. Kato, and T. Takahashi for helpful discussions, and M. Yamane for technical assistance.

Author Contributions

Conceived and designed the experiments: MI NS HS. Performed the experiments: MI NS. Analyzed the data: MI NS DM HI HS. Contributed reagents/materials/analysis tools: J. Mitsui MT J. Mineno. Contributed to the writing of the manuscript: MI NS.

References

1. Vaha-Koskela MJ, Heikkila JE, Hinkkanen AE (2007) Oncolytic viruses in cancer therapy. Cancer Lett 254: 178–216.
2. Breitbach CJ, Reid T, Burke J, Bell JC, Kirn DH (2010) Navigating the clinical development landscape for oncolytic viruses and other cancer therapeutics: no shortcuts on the road to approval. Cytokine Growth Factor Rev 21: 85–89.
3. Eager RM, Nemunaitis J (2011) Clinical development directions in oncolytic viral therapy. Cancer Gene Ther 18: 305–317.
4. Kim JH, Oh JY, Park BH, Lee DE, Kim JS, et al. (2006) Systemic armed oncolytic and immunologic therapy for cancer with JX-594, a targeted poxvirus expressing GM-CSF. Mol Ther 14: 361–370.
5. Park BH, Hwang T, Liu TC, Sze DY, Kim JS, et al. (2008) Use of a targeted oncolytic poxvirus, JX-594, in patients with refractory primary or metastatic liver cancer: a phase I trial. Lancet Oncol 9: 533–542.
6. Merrick AE, Ilett EJ, Melcher AA (2009) JX-594, a targeted oncolytic poxvirus for the treatment of cancer. Curr Opin Investig Drugs 10: 1372–1382.
7. Hwang TH, Moon A, Burke J, Ribas A, Stephenson J, et al. (2011) A mechanistic proof-of-concept clinical trial with JX-594, a targeted multi-mechanistic oncolytic poxvirus, in patients with metastatic melanoma. Molecular Ther 19: 1913–1922.
8. Breitbach CJ, Burke J, Jonker D, Stephenson J, Haas AR, et al. (2011) Intravenous delivery of a multi-mechanistic cancer-targeted oncolytic poxvirus in humans. Nature 477: 99–102.
9. Liu BL, Robinson M, Han ZQ, Branston RH, English C, et al. (2003) ICP34.5 deleted herpes simplex virus with enhanced oncolytic, immune stimulating, and anti-tumour properties. Gene Ther 10: 292–303.
10. Kaufman HL, Kim DW, DeRaffele G, Mitcham J, Coffin RS, et al. (2010) Local and distant immunity induced by intralesional vaccination with an oncolytic herpes virus encoding GM-CSF in patients with stage IIIc and IV melanoma. Ann Surg Oncol 17: 718–730.
11. Kaufman HL, Bines SD (2010) OPTIM trial: a Phase III trial of an oncolytic herpes virus encoding GM-CSF for unresectable stage III or IV melanoma. Future Oncol 6: 941–949.
12. Andtbacka RHI, Collichio FA, Amatruda T, Senzer NN, Chesney J, et al. (2013) OPTiM: A randomized phase III trial of talimogene laherparepvec (T-VEC) versus subcutaneous (SC) granulocyte-macrophage colony-stimulating factor (GM-CSF) for the treatment (tx) of unresected stage IIIB/C and IV melanoma. J Clin Oncol 31: suppl; abstr LBA9008.
13. Campadelli-Fiume G, De Giovanni C, Gatta V, Nanni P, Lollini PL, et al. (2011) Rethinking herpes simplex virus: the way to oncolytic agents. Rev Med Virol 21: 213–226.
14. Nishiyama Y, Kimura H, Daikoku T (1991) Complementary lethal invasion of the central nervous system by nonneuroinvasive herpes simplex virus types 1 and 2. J Virol 65: 4520–4524.
15. Mori I, Liu B, Goshima F, Ito H, Koide N, et al. (2005) HF10, an attenuated herpes simplex virus (HSV) type 1 clone, lacks neuroinvasiveness and protects mice against lethal challenge with HSV types 1 and 2. Microbes Infect 7: 1492–1500.
16. Nakao A, Kimata H, Imai T, Kikumori T, Teshigahara O, et al. (2004) Intratumoral injection of herpes simplex virus HF10 in recurrent breast cancer. Ann Oncol 15: 988–989.
17. Fujimoto Y, Mizuno T, Sugiura S, Goshima F, Kohno S, et al. (2006) Intratumoral injection of herpes simplex virus HF10 in recurrent head and neck squamous cell carcinoma. Acta Otolaryngol 126: 1115–1117.
18. Kimata H, Imai T, Kikumori T, Teshigahara O, Nagasaka T, et al. (2006) Pilot study of oncolytic viral therapy using mutant herpes simplex virus (HF10) against recurrent metastatic breast cancer. Ann Surgical Oncol 13: 1078–1084.
19. Nakao A, Kasuya H, Sahin TT, Nomura N, Kanzaki A, et al. (2011) A phase I dose-escalation clinical trial of intraoperative direct intratumoral injection of HF10 oncolytic virus in non-resectable patients with advanced pancreatic cancer. Cancer Gene Ther 18: 167–175.
20. Kohno SI, Luo C, Nawa A, Fujimoto Y, Watanabe D, et al. (2007) Oncolytic virotherapy with an HSV amplicon vector expressing granulocyte-macrophage colony-stimulating factor using the replication-competent HSV type 1 mutant HF10 as a helper virus. Cancer Gene Ther 14: 918–926.
21. Goshima F, Esaki S, Luo C, Kamakura M, Kimura H, et al. (2014) Oncolytic viral therapy with a combination of HF10, a herpes simplex virus type 1 variant and granulocyte-macrophage colony-stimulating factor for murine ovarian cancer. Int J Cancer 134: 2865–2877.
22. Nocentini G, Giunchi L, Ronchetti S, Krausz LT, Bartoli A, et al. (1997) A new member of the tumor necrosis factor/nerve growth factor receptor family inhibits T cell receptor-induced apoptosis. Proc Natl Acad Sci USA 94: 6216–6221.
23. Pardoll DM (2012) The blockade of immune checkpoints in cancer immunotherapy. Nat Rev Cancer 12: 252–264.
24. McHugh RS, Whitters MJ, Piccirillo CA, Young DA, Shevach EM, et al. (2002) CD4(+)CD25(+) immunoregulatory T cells: gene expression analysis reveals a functional role for the glucocorticoid-induced TNF receptor. Immunity 16: 311–323.
25. Shimizu J, Yamazaki S, Takahashi T, Ishida Y, Sakaguchi S (2002) Stimulation of CD25(+)CD4(+) regulatory T cells through GITR breaks immunological self-tolerance. Nat Immunol 3: 135–142.
26. Cote AL, Zhang P, O'Sullivan JA, Jacobs VL, Clemis CR, et al. (2011) Stimulation of the glucocorticoid-induced TNF receptor family-related receptor on CD8 T cells induces protective and high-avidity T cell responses to tumor-specific antigens. J Immunol 186: 275–283.
27. Nishikawa H, Kato T, Hirayama M, Orito Y, Sato E, et al. (2008) Regulatory T cell-resistant CD8+ T cells induced by glucocorticoid-induced tumor necrosis factor receptor signaling. Cancer Res 68: 5948–5954.
28. Rosenzweig M, Ponte J, Apostolou I, Doty D, Guild J, et al. (2010) Development of TRX518, an aglycosyl humanized monoclonal antibody (Mab) agonist of huGITR. J Clin Oncol 28: suppl; abstr e13028.
29. Takai T, Li M, Sylvestre D, Clynes R, Ravetch JV (1994) FcR gamma chain deletion results in pleiotrophic effector cell defects. Cell 76: 519–529.
30. Lerner WA, Pearlstein E, Ambrogio C, Karpatkin S (1983) A new mechanism for tumor induced platelet aggregation. Comparison with mechanisms shared by other tumor with possible pharmacologic strategy toward prevention of metastases. Int J Cancer 31: 463–469.
31. Muraoka D, Kato T, Wang L, Maeda Y, Noguchi T, et al. (2010) Peptide vaccine induces enhanced tumor growth associated with apoptosis induction in CD8+ T cells. J Immunol 185: 3768–3776.
32. Ikeda H, Ohta N, Furukawa K, Miyazaki H, Wang L, et al. (1997) Mutated mitogen-activated protein kinase: a tumor rejection antigen of mouse sarcoma. Proc Natl Acad Sci USA 94: 6375–6379.
33. Huang AY, Gulden PH, Woods AS, Thomas MC, Tong CD, et al. (1996) The immunodominant major histocompatibility complex class I-restricted antigen of a murine colon tumor derives from an endogenous retroviral gene product. Proc Natl Acad Sci USA 93: 9730–9735.
34. Mitsui J, Nishikawa H, Muraoka D, Wang L, Noguchi T, et al. (2010) Two distinct mechanisms of augmented antitumor activity by modulation of immunostimulatory/inhibitory signals. Clin Cancer Res 16: 2781–2791.

35. Hamid O, Robert C, Daud A, Hodi FS, Hwu WJ, et al. (2013) Safety and tumor responses with lambrolizumab (anti-PD-1) in melanoma. N Engl J Med 369: 134–144.
36. Postow MA, Luke JJ, Bluth MJ, Ramaiya N, Panageas KS, et al. (2013) Ipilimumab for patients with advanced mucosal melanoma. Oncologist 18: 726–732.
37. Ribas A, Kefford R, Marshall MA, Punt CJ, Haanen JB, et al. (2013) Phase III randomized clinical trial comparing tremelimumab with standard-of-care chemotherapy in patients with advanced melanoma. J Clin Oncol 31: 616–622.
38. Weber JS, Dummer R, de Pril V, Lebbe C, Hodi FS (2013) Patterns of onset and resolution of immune-related adverse events of special interest with ipilimumab: detailed safety analysis from a phase 3 trial in patients with advanced melanoma. Cancer 119: 1675–1682.
39. Ko K, Yamazaki S, Nakamura K, Nishioka T, Hirota K, et al. (2005) Treatment of advanced tumors with agonistic anti-GITR mAb and its effects on tumor-infiltrating Foxp3+CD25+CD4+ regulatory T cells. J Exp Med 202: 885–891.
40. Robert C, Thomas L, Bondarenko I, O'Day S, Weber J, et al. (2011) Ipilimumab plus dacarbazine for previously untreated metastatic melanoma. N Engl J Med 364: 2517–2526.
41. Brahmer JR, Tykodi SS, Chow LQ, Hwu WJ, Topalian SL, et al. (2012) Safety and activity of anti-PD-L1 antibody in patients with advanced cancer. N Engl J Med 366: 2455–2465.
42. Topalian SL, Hodi FS, Brahmer JR, Gettinger SN, Smith DC, et al. (2012) Safety, activity, and immune correlates of anti-PD-1 antibody in cancer. N Engl J Med 366: 2443–2454.
43. Curiel TJ, Coukos G, Zou L, Alvarez X, Cheng P, et al. (2004) Specific recruitment of regulatory T cells in ovarian carcinoma fosters immune privilege and predicts reduced survival. Nat Med 10: 942–949.
44. Wolf D, Wolf AM, Rumpold H, Fiegl H, Zeimet AG, et al. (2005) The expression of the regulatory T cell-specific forkhead box transcription factor FoxP3 is associated with poor prognosis in ovarian cancer. Clin Cancer Res 11: 8326–8331.
45. Wang W, Hodkinson P, McLaren F, MacKinnon A, Wallace W, et al. (2012) Small cell lung cancer tumour cells induce regulatory T lymphocytes, and patient survival correlates negatively with FOXP3+ cells in tumour infiltrate. Int J Cancer 131: E928–937.
46. Francisco LM, Salinas VH, Brown KE, Vanguri VK, Freeman GJ, et al. (2009) PD-L1 regulates the development, maintenance, and function of induced regulatory T cells. J Exp Med 206: 3015–3029.
47. Simpson TR, Li F, Montalvo-Ortiz W, Sepulveda MA, Bergerhoff K, et al. (2013) Fc-dependent depletion of tumor-infiltrating regulatory T cells co-defines the efficacy of anti-CTLA-4 therapy against melanoma. J Exp Med 210: 1695–1710.
48. Cohen AD, Diab A, Perales MA, Wolchok JD, Rizzuto G, et al. (2006) Agonist anti-GITR antibody enhances vaccine-induced CD8(+) T-cell responses and tumor immunity. Cancer Res 66: 4904–4912.
49. Cohen AD, Schaer DA, Liu C, Li Y, Hirschhorn-Cymmerman D, et al. (2010) Agonist anti-GITR monoclonal antibody induces melanoma tumor immunity in mice by altering regulatory T cell stability and intra-tumor accumulation. PLoS One 5: e10436.
50. Li YQ, Liu FF, Zhang XM, Guo XJ, Ren MJ, et al. (2013) Tumor secretion of CCL22 activates intratumoral Treg infiltration and is independent prognostic predictor of breast cancer. PLoS One 8: e76379.
51. Imai N, Ikeda H, Tawara I, Wang L, Wang L, et al. (2009) Glucocorticoid-induced tumor necrosis factor receptor stimulation enhances the multifunctionality of adoptively transferred tumor antigen-specific CD8+ T cells with tumor regression. Cancer Sci 100: 1317–1325.
52. La S, Kim E, Kwon B (2005) In vivo ligation of glucocorticoid-induced TNF receptor enhances the T-cell immunity to herpes simplex virus type 1. Exp Mol Med 37: 193–198.